Final Technical Report

USGS Award #G20AP00040 and #G20AP00041

Characterization of soil amplification in glaciated terrains: Collaborative Research with Tufts University and Boston College

Laurie G. Baise, Professor and Chair
Dept. Civil and Env. Engineering, Tufts University, 200 College Ave, Medford, MA, 02155
617-627-2211, 617-627-3994, laurie.baise@tufts.edu

John Ebel, Senior Research Scientist
Weston Observatory, Weston Observatory, Department of Earth and Environmental Sciences, Boston College, 381 Concord Rd., Weston, MA 02493, USA, ebel@bc.edu

Marshall Pontrelli, Graduate Student Researcher
Dept. Civil and Env. Engineering, Tufts University, 200 College Ave, Medford, MA, 02155

Sean Kondas, Graduate Student Researcher
Weston Observatory, Department of Earth and Environmental Sciences, Boston College, 381 Concord Rd., Weston, MA 02493, USA

Ian Cooper, Graduate Student Researcher
Weston Observatory, Department of Earth and Environmental Sciences, Boston College, 381 Concord Rd., Weston, MA 02493, USA

"This material is based upon work supported by the U.S. Geological Survey under Grant No. G20AP00040 and G20AP00041."

June 1, 2020 – December 31, 2021

Abstract

In this research, we develop regional surficial geology-based maps to characterize soil amplification in the New England region. We prepare a spatial database of 1625 HVSR measurements from ambient noise measurements, collected from the literature, and our own field campaign of 487 measurements. Using Nakamura's HVSR technique (Nakamura, 1989), we compute the fundamental frequency, f_0, which is a known site characterization parameter associated with the frequency of resonance. Using surficial geologic units from the Conterminous US surficial geology map (Soller et al. 2009) and based on the methodology that Wills and Clahan (2006) used to group *Vs30* measurements, we provide f_0 summary statistics for each geologic unit in New England. Some surficial geologic units are combined using depositional environment and depositional thickness where we have few f_0 stations. We calculate measures of central tendency and dispersion for each unit. Using this approach, we observe that thick proglacial sediments on Cape Cod and Long Island tend to have the lowest f_0 measurements, consistent with a deep soil profile. We also see that the marine clays in Boston, the coast of Lake Champlain and the alluvial sediments in the Connecticut River Valley tend to have the next lowest frequencies, which we attribute to sediment thicknesses less than what is observed on Cape Cod and Long Island. Finally, we observe that the blanket of till covering the majority of New England tends to have high f_0 values in the region, indicating shallow sediments. We also establish estimates of sediment shear-wave velocity for each of the surficial geologic units based on a combination of in-situ measurements, engineering judgement, and expert opinion. Using the common relationship of $f_0 = Vs/4d$ which relates f_0 to shear wave velocity and depth, we relate f_0 distributions to soil amplification and site response prediction in New England. Additionally, we calculate κ_0 values for regional seismic stations on rock and sediment sites in New England. κ_0 values are consistently less than 0.02 s throughout most of New England and New York, reaching above 0.30 s near the St. Lawrence River northeast of Quebec City.

Introduction

The horizontal-to-vertical spectral ratio (HVSR, Nakamura, 1989) has been used to characterize site response in high impedance contrast areas (Baise et al. 2016, Braganza et al. 2016). Nakamura (1989) showed that the fundamental resonance peak, f_0, of the HVSR is empirically similar to the fundamental peak of the SH1D transfer function and thus can be used to estimate site amplification effects. The SH1D transfer function is a theoretical wave propagation model that assumes 1) vertically propagating shear waves through 2) laterally homogenous soil layers that have 3) frequency independent damping and 4) strain independent shear moduli. It requires an input soil profile of layer shear wave velocities, thicknesses, densities and damping values and outputs the amplification ratio of the free surface to the soil profile base as a function of frequency. The common relationship, $f_0 = Vs/4d$, provides a simple way of relating f_0 to shear wave velocity and depth. Researchers commonly use the HVSR to estimate site response in resonant sediments because it is inexpensive and requires relatively simple processing steps (Lermo and Chávez-Garcia, 1993; Carpenter et al. 2018; Zhu et al. 2020). Additionally, researchers have been interested in the use of f_0 as a predictor of site response and as a site term in ground motion models (Braganza et al. 2016, Gallipoli and Mucciarelli 2009, Pitilakis et al. 2019). Several researchers have shown that f_0 can complement and sometimes outperform *Vs30* in certain circumstances as a site parameter in ground motion models (Hassani and Atkinson 2016). f_0 is known to perform well in high impedance environments where the site response exhibits a strongly resonant behavior.

Baise et al. (2016) showed that the Boston Basin has a high impedance contrast beneath the surficial sediments and displays significant site amplification. In related work, Yilar et al. (2017) presented an HVSR microzonation study in the Boston basin and validated the ability of the HVSR method (Nakamura, 1989)

to perform well in regions underlain by artificial fill, marine clays, and glaciofluvial sediments (Yilar et al. 2017). Additionally, Hassani and Atkinson (2016) showed that f_0 works well as a site response predictor in eastern Canada due to the high impedance contrasts in the area. High near-surface impedance contrasts are common throughout New England due to the soft overburden layers found in several typical glacial geologic environments, specifically outwash, glacial lake deposits, marine clays, and flood plain alluvium that overlie the bedrock. Additionally, New England basement rock has high velocities (e.g. 2000-3000 m/s) and thus consistently exhibits high impedance contrasts throughout New England.

In this work, we use f_0 derived from the HVSR to map site effects across New England by grouping f_0 values by their geologic unit, similar to the methodology used in Wills and Clahan (2006) which they applied to grouping *Vs30* values in the state of California. We also develop estimates of sediment shear-wave velocity by surficial geologic unit to relate f_0 to sediment thickness. The resulting f_0 map of New England can be used for regional seismic hazard assessments. f_0 and *Vs30* can be used as site parameters in ground-motion models. Future iterations of design code may also use f_0 in parallel with *Vs30* to determine the soil amplification at a site.

Another relevant site parameter is f_{max}. Anderson and Hough (1984) showed that the amplitude spectra of accelerograms decay with increasing frequency above some frequency called f_{max}. This high-frequency amplitude decay apparently is caused by attenuation effects in the near-surface (uppermost 10s of meters) beneath the accelerograph station. For a given seismic station, at frequencies above f_{max} on a semilog plot the amplitude spectrum is linear with a negative slope called κ. This slope is greater when the station is at a greater distance from the seismic source. From the κ values as a function of epicentral distance, a line is fit to the values and the intercept of the line is called κ_0, which is considered the intrinsic κ value for the site. There is broad interest in the determinations of κ_0 for sites in all parts of the world where seismic hazard analyses are being carried out (Chandler et al., 2006).

For hard-rock sites in eastern North America, past studies with a focus on eastern Canada have determined a regional minimum κ_0 of 0 and a maximum value of about 0.01 (e.g., Atkinson, 1996). Probabilistic seismic hazard analysis projects require clearly defined reference rock parameters such as κ_0 for hazard computations (Van Houtte et al., 2011), and it is also necessary to determine κ_0 values for sites with till and soil cover in the northeastern U.S. (Laurendeau et al., 2013) In this part of this project, we have investigated the κ_0 values from accelerometer records for glaciated hard-rock sites as well as for sites with glacial and quaternary sediments throughout the northeastern United States, a region for which few κ_0 have been previously found. We determined κ_0 by determining a linear least-squares fit to acceleration amplitude spectra at high frequencies in frequency/log-amplitude space (Anderson and Hough, 1984). The results of this work are to provide information on the κ_0 scaling term in ground-motion models (GMMs), such as those proposed by Hassani and Atkinson (2018), to estimate best-fit values for the terrain-specific conditions of each instrumented site in the northeastern U.S.

Data and methods

Conterminous US surficial geology map

The US conterminous surficial geology map is a 1:5,000,000 scale map compiled through a process involving the communication with state geological surveys to identify priority geologies and to develop a general overview of each state's geology (Soller et al. 2009). Prior to the publication of the 1:5,000,000 scale map, the best map available for surficial materials in the US was at 1:7,000,000 scale. The compiler's strategy was to incorporate state-scale geologic maps where available directly into the conterminous map and to develop generalizations where these maps were not available. The US states where surficial maps existed were all in the western US, and thus the northeastern states were all generalized in this country-

scale map. The authors of Soller et al. (2009) are candid about the generalized nature of the map, saying "Because of its generalized unit descriptions, regional scale, and incomplete integration across the map area, this map is not intended for decision making at the local, site-specific level." (Soller and Reheis, 2004). We acknowledge this broad generalization, and in our classifications in this study we regard each f_0 distribution that we develop as a general description of the large-scale distribution of the significant surficial geologic units in New England but not as a sufficient description for site scale interpretations.

When the Conterminous map of Soller et al. (2009), is clipped to the New England region (Figure 1), the resulting map contains 20 surficial geologic units representing 3 different thicknesses, 8 depositional environments and 8 grain sizes (Table 1). Most of the map's area is dominated by some form of glacial till with extensive marine clay deposits (classified as "proglacial sediments, fine-grained") on the coast of Maine down to Boston and along the coast of Lake Champlain in Vermont. These marine clay deposits on the Maine coast are the "Presumpscot formation", where in the Boston basin they are the "Boston Blue Clay" and on the Lake Champlain coast they are the "Champlain Sea Sediments". On Cape Cod and Long Island there are extensive "thick proglacial sediments" that are large, deep terminal moraines that represent the southernmost extent of the Wisconsin glaciation. Finally, a large band of "Alluvial sediments" are in central Massachusetts and Connecticut, bounded by thin proglacial sediments (clay). These are the Connecticut River valley flood-plain alluvial deposits sitting within the Glacial Lake Hitchcock clay sediments.

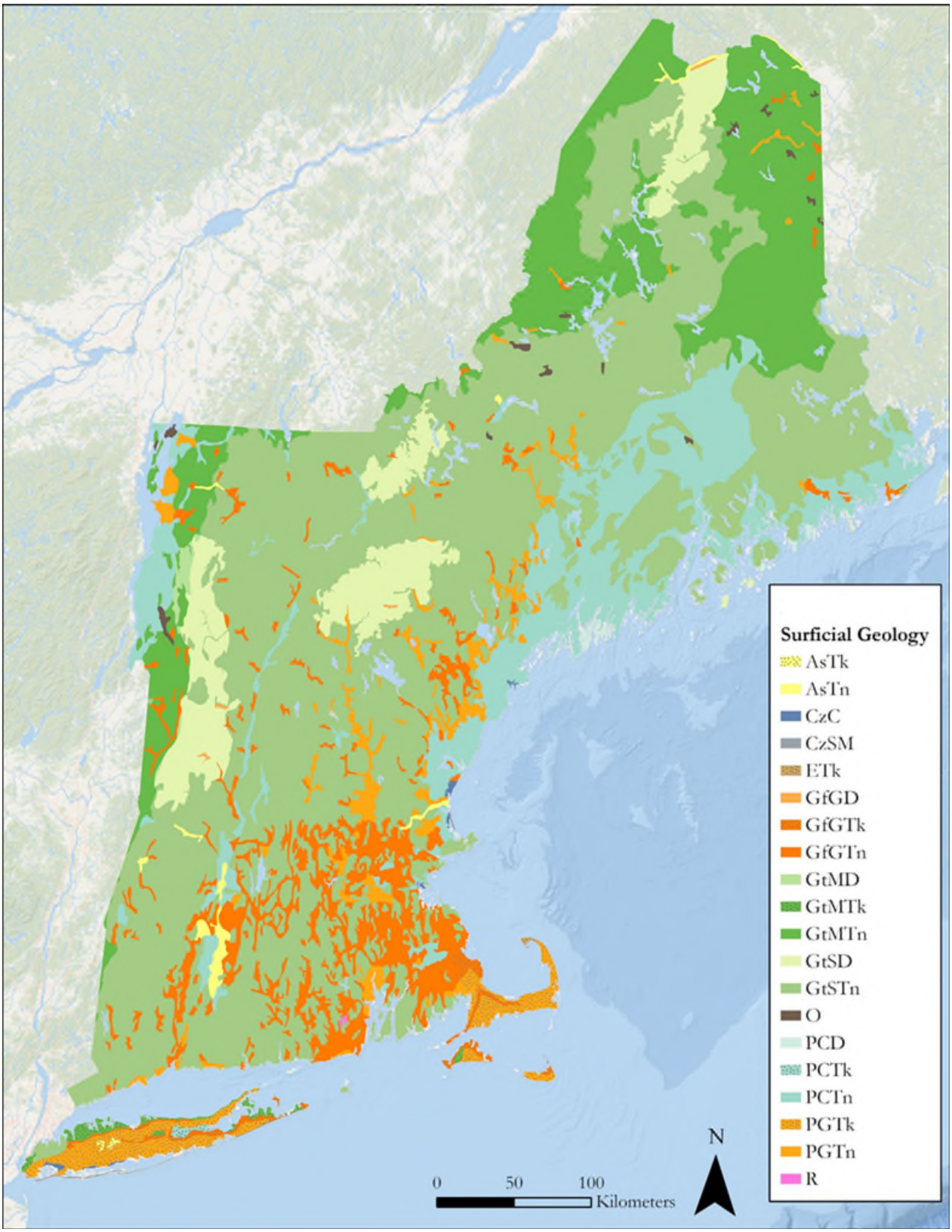

Figure 1. Conterminous map of the surficial geology in New England (Soller et al. 2009). The label descriptions are in Table 1.

Table 1. Surficial geologic units and their respective labels indicating thickness, depositional environment, and grain size from the Conterminous map (Soller et al. 2009).

Surficial unit	Label	Thickness	Depositional environment	Grain size
Alluvial sediments, thick	AsTk	Thick	Alluvial	
Alluvial sediments, thin	AsTn	Thin	Alluvial	
Coastal zone sediments, mostly fine-grained	CzC	Thin	Coastal	Mostly fine-grained
Coastal zone sediments, mostly medium-grained	CZzSM	Thin	Coastal	Mostly medium-grained
Eolian sediments, mostly dune sand, thick	ETk	Thick	Eolian	Mostly dune sand
Glacial till sediments, mostly sandy, discontinuous	GtSD	Discontinuous	Glacial till	Mostly sandy
Glacial till sediments, mostly sandy, thin	GtSTn	Thin	Glacial til	Mostly sandy
Glacial till sediments, mostly silty, discontinuous	GtMD	Discontinuous	Glacial till	Mostly silty
Glacial till sediments, mostly silty, thick	GtMTk	Thick	Glacial till	Mostly silty
Glacial till sediments, mostly silty, thin	GtMTn	Thin	Glacial till	Mostly silty
Glaciofluvial ice-contact sediments, mostly sand and gravel, discontinuous	GfGD	Discontinuous	Glaciofluvial	Mostly sand and gravel
Glaciofluvial ice-contact sediments, mostly sand and gravel, thick	GfGTk	Thick	Glaciofluvial	Mostly sand and gravel
Glaciofluvial ice-contact sediments, mostly sand and gravel, thin	GfGTn	Thin	Glaciofluvial	Mostly sand and gravel
Organic-rich muck and peat, thin	O	Thin	Organic-rich mich and peat	Peat
Proglacial sediments, mostly coarse-grained, thick	PGTk	Thick	Proglacial	Mostly coarse-grained
Proglacial sediments, mostly coarse-grained, thin	PGTn	Thin	Proglacial	Mostly coarse-grained
Proglacial sediments, mostly fine grained, discontinuous	PCD	Discontinuous	Proglacial	Mostly fine-grained
Proglacial sediments, mostly fine grained, thick	PCTk	Thick	Proglacial	Mostly fine-grained
Proglacial sediments, mostly fine grained, thin	PCTn	Thin	Proglacial	Mostly fine-grained
Residual materials developed in igneous and metamorphic rocks	R	Discontinuous	Residual materials	
Water	W			

f_0 database

In this project, we characterize site response primarily by f_0. To develop our f_0 database, we first compiled HVSR measurements from prior projects. Yilar et al. (2017) included 570 f_0 measurements in the greater Boston area. Fairchild et al. (2013) included 198 HVSR measurements in Cape Cod that were collected as part of groundwater study. Steve Mabee (Massachusetts geological survey, personal communication) provided 545 f_0 measurements across Massachusetts and in the Connecticut River Valley. The existing f_0 locations were spread across Massachusetts and then clustered on Cape Cod, in greater Boston, and through the Connecticut River Valley. To complement these data, we collected 487 more f_0 measurements with a field campaign aimed to cover New England using major highways in New England and targeting geologic deposits where we expected local amplification of seismic shaking. With these goals in mind, the field collection targeted Long Island, the southern (Connecticut-portion) of the Connecticut River Valley, the Presumpscot clays in coastal Maine and the Champlain Sea Sediments in northwestern Vermont. Additionally, we calculated f_0 values at all of the permanent seismic stations in New England and included them in the study. Figure 2 shows the f_0 locations included in this study.

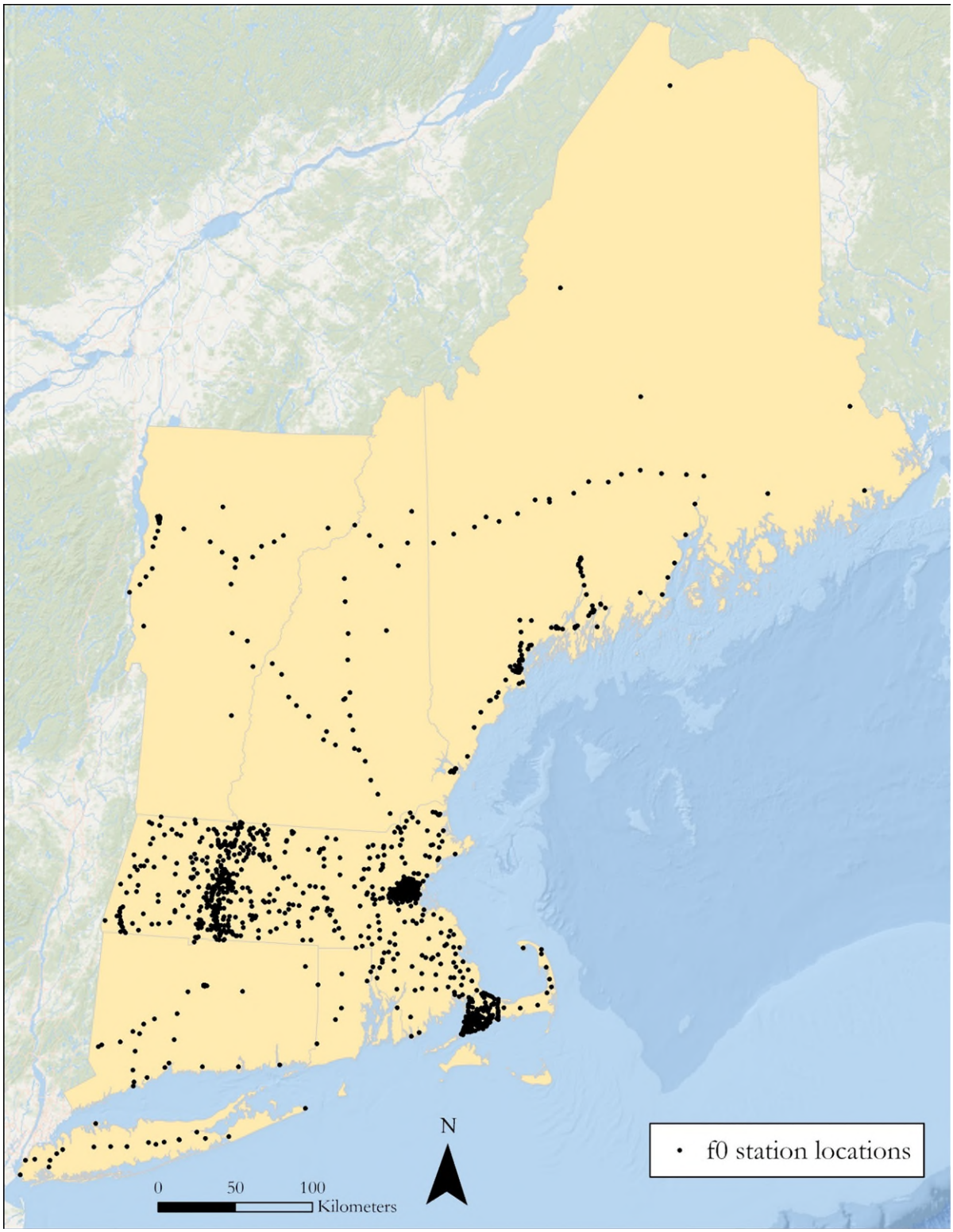

Figure 2. Spatial distribution of the f_0 database compiled in this study. The long north-south trending lines in the northern states are collection lines along interstate highways and the east-west transect across VT, NH and ME, is route 2, running from the Berkshires through the Connecticut River Valley, the White Mountains and into Maine along the Androscoggin River.

We processed the data using Nakamura's HVSR technique, first collecting 15 minutes of ambient noise data sampling at 100 Hz using a CMG-40t broadband seismometer and a Reftek 130 digitizer (Figure 3a) placed on concrete or asphalt - we found that coupling the instrument on soft ground yielded unreliable results (SESAME, 2004 a and b; Yilar et al. 2017). We filtered the noise using a four-pole Butterworth filter with a low corner frequency of 0.1 Hz and a high corner frequency of 49 Hz and then divided the resulting time series into twenty windows, each of forty seconds duration, and with one second window spacing. After windowing the data, we computed the Fourier amplitude spectra (FAS) of each window and each component, smoothed the spectra with a 0.5 Hz wide smoothing filter, and combined the horizontal components using the geometric mean (Figure 3b). We then divided the horizontal component by the vertical component of each window to get 20 HVSR curves (Figure 3c). Finally, we compute the median and standard deviation HVSR curve (Figure 3d) from all the windows using the maximum likelihood estimator:

$$HVSR_{med}(f) = exp\left(\frac{1}{n}\sum_{i=1}^{n}\ln[HVSR_i(f)]\right) \quad (1)$$

where $HVSR_i(f)$ is the $HVSR(f)$ for i = 1,…,n windows with standard deviation:

$$\sigma_{ln}(f) = \sqrt{\frac{1}{n}\sum_{i=1}^{n}(\ln[HVSR_i(f)] - \ln[HVSR(f)])^2} \quad (2)$$

(Thompson et al. 2012) (Fig. 3).

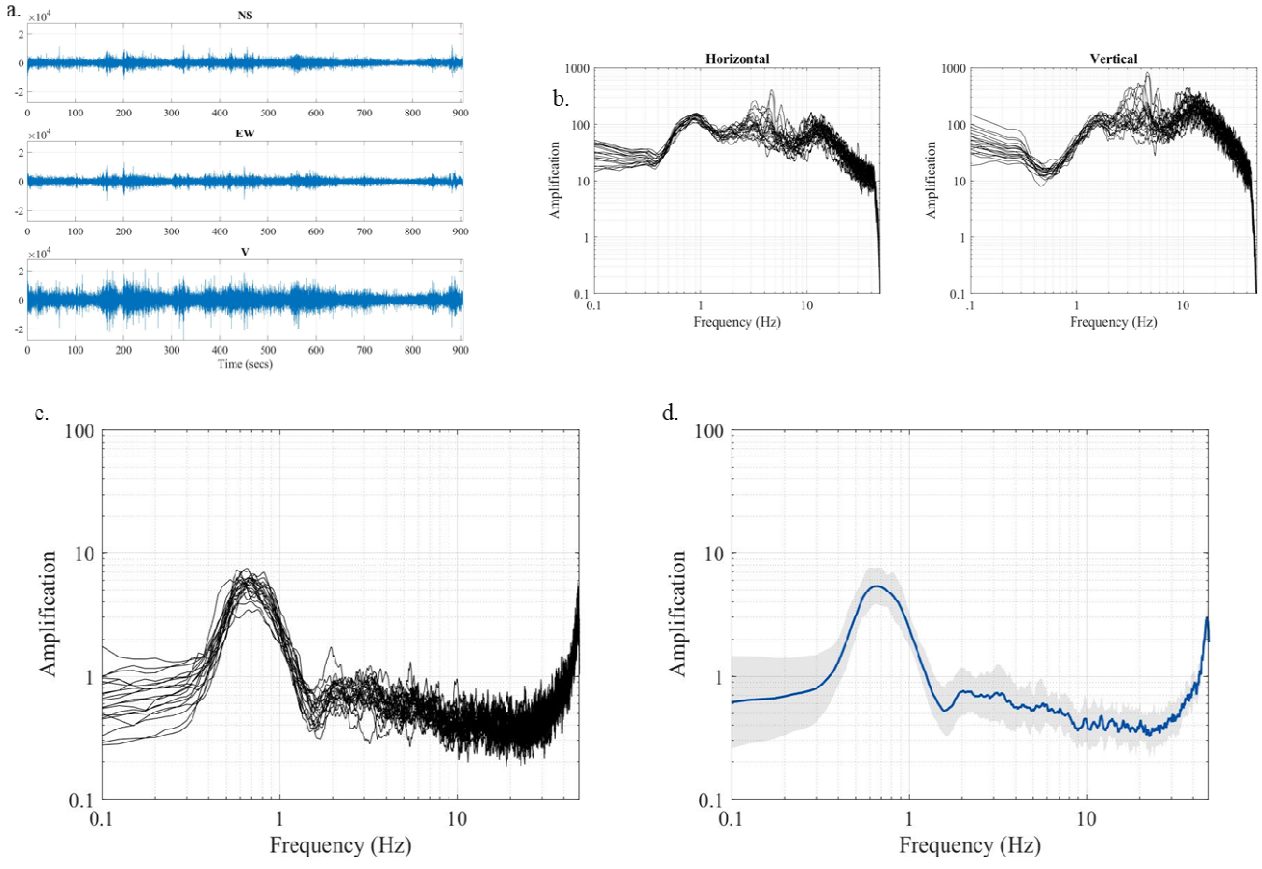

Figure 3. Processing steps for computing HVSR curves, a) time series, b) Fourier amplitude spectra (horizontal and vertical), c) individual HVSR curves and d) final averaged HVSR curve.

Our f_0 database consists of 1625 points. In the analysis, we work in natural log-units and then convert back to natural units of Hz when presenting data on maps and in tables. The summary statistics of the f_0 database are shown in Table 2 in both logarithmic and natural units. We calculate the median and first and third quartiles in logarithmic units and then convert to natural units. We then calculate the interquartile range (IQR) by subtracting the natural 25th percentile value from the natural 75th percentile. The median of the dataset is 3.05 Hz, the 25th percentile is 1.55 Hz and the 75th percentile is 6.82 Hz.

Table 2. Properties of the distribution of f_0 measurements in the database.

Measurement	Logarithmic units	Natural units
Median	1.11	3.05
IQR	1.48	5.27
25th percentile	0.43	1.55
75th percentile	1.92	6.82
Mean	1.22	3.40
Standard deviation	1.02	2.77

f_0 by surficial geologic unit based on conterminous geology map

Beginning with the conterminous US map (Soller et al., 2009) clipped to the New England region including Long Island (Figure 1), we performed a spatial join with the f_0 database and counted the number of f_0 stations in each surficial unit, and then computed the IQR and median of the f_0 distribution within each of the surficial units (Table 3). In Table 3, only the top 8 units have enough f_0 stations from which we can confidently calculate summary statistics. To account for the surficial units without many f_0 stations (the bottom 12 units in Table 3), we combined them into the categories of the top 8 units which have enough f_0 stations. Table 4 shows how we grouped and renamed the units in Table 3. All the "thick" surficial geologic units without many points are located on Cape Cod or Long Island. In fact, all the "thick" classified units in the conterminous map are on Cape Cod and Long Island (Figure 4). These thick units likely have similar amplifying characters (depth and shear-wave velocities) to the rest of the units on Cape Cod and Long Island. Thus, we combined "proglacial sediments, mostly fine-grained, thick", "Alluvial sediments, thick", "Glacial till sediments, mostly silty, thick", and "Eolian sediments, mostly dune sand, thick" and "Proglacial sediments, mostly coarse grained, thick" into one category. We categorized both the thin and discontinuous glacial till with "glacial till sediments, mostly sandy, thin" because all the thin the glacial till units likely have high velocities and are thin deposits. We categorized "coastal zone sediments, mostly medium-grained" and "coastal zone sediments mostly fine-grained" together since both are coastal zone sediments and are likely to have similar ground amplification characteristics. We also kept "residual materials, developed in igneous and metamorphic rock" and "organic-rich muck and peat" (Soller et al. 2009_as their own categories even though there are no f_0 stations within their areas, but they cover a very small area on the map and have easily interpretable site response characteristics from their geology - we interpreted these units as site classes "A" and "E", respectively. With these new geologic classifications, we perform another spatial join and calculate the number of stations, IQR and median on each of the newly classified units (Table 5, Figure 5).

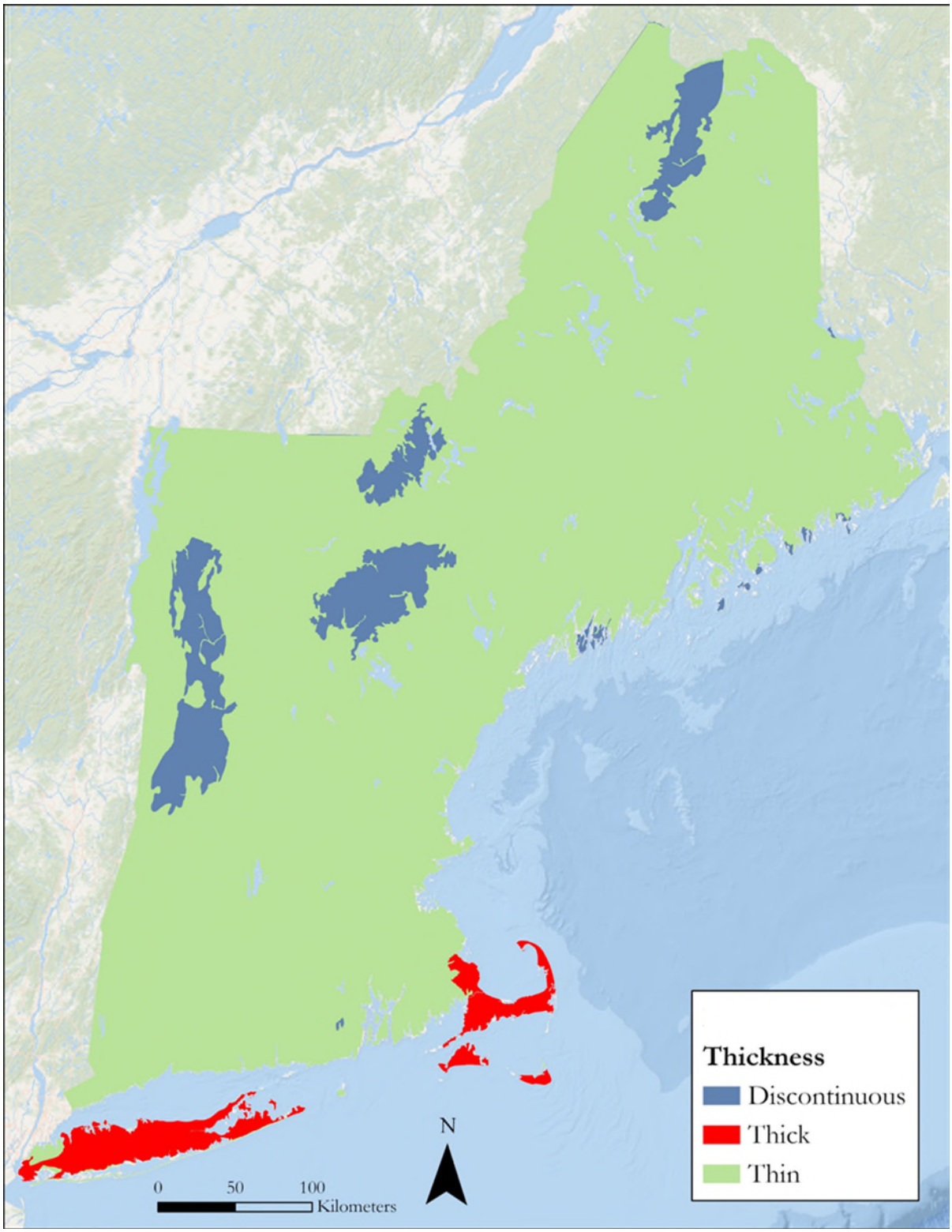

Figure 4. Conterminous map overburden thicknesses. Note how the thick overburden classification is entirely on Cape Cod and Long Island, how the discontinuous classification is concentrated in the mountainous areas (the Green and White Mountains) and how the thin classification is in the rest of New England.

Table 3. Surficial geologic units spatial joined to the f_0 stations with f_0 medians and IQR2 calculated from the distribution of f_0 points within in each unit.

Surficial unit	Thickness	Depositional environment	Grain size	# Stations	Median (Hz)	IQR (Hz)
Glaciofluvial ice-contact sediments, mostly sand and gravel, thin	Thin	Glaciofluvial	Mostly sand and gravel	461	4.00	6.60
Proglacial sediments, mostly fine grained, thin	Thin	Proglacial	Mostly fine-grained	381	2.70	3.65
Glacial till sediments, mostly sandy, thin	Thin	Glacial till	Mostly sandy	353	6.25	10.30
Proglacial sediments, mostly coarse-grained, thick	Thick	Proglacial	Mostly coarse-grained	174	1.03	0.32
Proglacial sediments, mostly coarse-grained, thin	Thin	Proglacial	Mostly coarse-grained	74	3.70	3.47
Alluvial sediments, thin	Thin	Alluvial		62	1.83	1.59
Glaciofluvial ice-contact sediments, mostly sand and gravel, thick	Thick	Glaciofluvial	Mostly sand and gravel	32	1.06	0.23
Coastal zone sediments, mostly fine-grained	Thin	Coastal	Mostly fine-grained	26	3.31	1.60
Glacial till sediments, mostly sandy, discontinuous	Discontinuous	Glacial till	Mostly sandy	4	2.75	2.01
Proglacial sediments, mostly fine grained, thick	Thick	Proglacial	Mostly fine-grained	3	0.48	0.04
Alluvial sediments, thick	Thick	Alluvial		2	0.46	0.08
Glacial till sediments, mostly silty, thick	Thick	Glacial till	Mostly silty	2	0.89	0.16
Glacial till sediments, mostly silty, thin	Thin	Glacial till	Mostly silty	2	3.17	0.25
Eolian sediments, mostly dune sand, thick	Thick	Eolian	Mostly dune sand	1	0.53	0.00
Coastal zone sediments, mostly medium-grained	Thin	Coastal	Mostly medium-grained	0		
Glacial till sediments, mostly silty, discontinuous	Discontinuous	Glacial till	Mostly silty	0		
Glaciofluvial ice-contact sediments, mostly sand and gravel, discontinuous	Discontinuous	Glaciofluvial	Mostly sand and gravel	0		
Organic-rich muck and peat, thin	Thin	Organic-rich mich and peat	Peat	0		
Proglacial sediments, mostly fine grained, discontinuous	Discontinuous	Proglacial	Mostly fine-grained	0		
Residual materials developed in igneous and metamorphic rocks	Discontinuous	Residual materials		0		

Table 4. Surficial geologic unit grouping based on the number of f_0 stations in the different units and the units' location and geology.

New surficial name	Surficial unit groups	Thickness
Glaciofluvial ice-contact sediments, thin	Glaciofluvial ice-contact sediments, mostly sand and gravel, thin; Glaciofluvial ice-contact sediments, mostly sand and gravel, discontinuous	Thin
Proglacial sediments, fine grained, thin	Proglacial sediments, mostly fine grained, thin; Proglacial sediments, mostly fine grained, discontinuous	Thin
Glacial till	Glacial till sediments, mostly sandy, thin; Glacial till sediments, mostly sandy, discontinuous; Glacial till sediments, mostly silty, thin; Glacial till sediments, mostly silty, discontinuous	Thin
Proglacial sediments, thick	Proglacial sediments, mostly coarse-grained, thick; Proglacial sediments, mostly fine grained, thick; Alluvial sediments, thick; Glacial till sediments, mostly silty, thick; Eolian sediments, mostly dune sand, thick	Thick
Proglacial sediments, coarse grained, thin	Proglacial sediments, mostly coarse-grained, thin	Thin
Alluvial sediments, thin	Alluvial sediments, thin	Thin
Glaciofluvial ice-contact sediments, thick	Glaciofluvial ice-contact sediments, mostly sand and gravel, thick	Thick
Coastal zone sediments	Coastal zone sediments, mostly fine-grained; Coastal zone sediments, mostly medium-grained	Thin
Organic-rich muck and peat, thin	Organic-rich muck and peat, thin	Thin
Residual materials	Residual materials developed in igneous and metamorphic rocks	Thin

Shear wave velocity estimates

There are tens of existing shear wave velocity profiles in the New England area, and we collected five more in this study, but the database does not yet have enough profiles to fill in the distributions of overburden average shear wave velocity using the same methodology that we use for f_0 in this study. We decided for this study to combine this profile information with local expert knowledge to develop the Vs_{avg} column in Table 5.

Table 5. Final output table for the f_0 stations joined to their respective merged surficial geologic units with calculated medians and IQRs of the distribution of f_0 values in each unit and estimates for average shear wave velocities.

Surficial unit	Thickness	# Stations	Median (Hz)*	IQR (HZ)*	Vs_{avg} (m/s)$^{\tau}$
Glaciofluvial ice-contact sediments, thin	Thin	461	4.00	6.60	220-300
Proglacial sediments, mostly fine grained, thin	Thin	381	2.70	3.65	150-220
Glacial till	Thin	359	6.16	10.15	300-500
Proglacial sediments, thick	Thick	182	1.03	0.28	180-250
Proglacial sediments, coarse-grained, thin	Thin	74	3.70	3.47	220-300
Alluvial sediments, thin	Thin	62	1.83	1.59	170-250
Glaciofluvial ice-contact sediments, thick	Thick	32	1.06	0.23	180-250
Coastal zone sediments, mostly fine-grained	Thin	26	3.31	1.60	150-220

* Columns calculated from data in this study
$^{\tau}$ Columns estimated from data and local expertise.

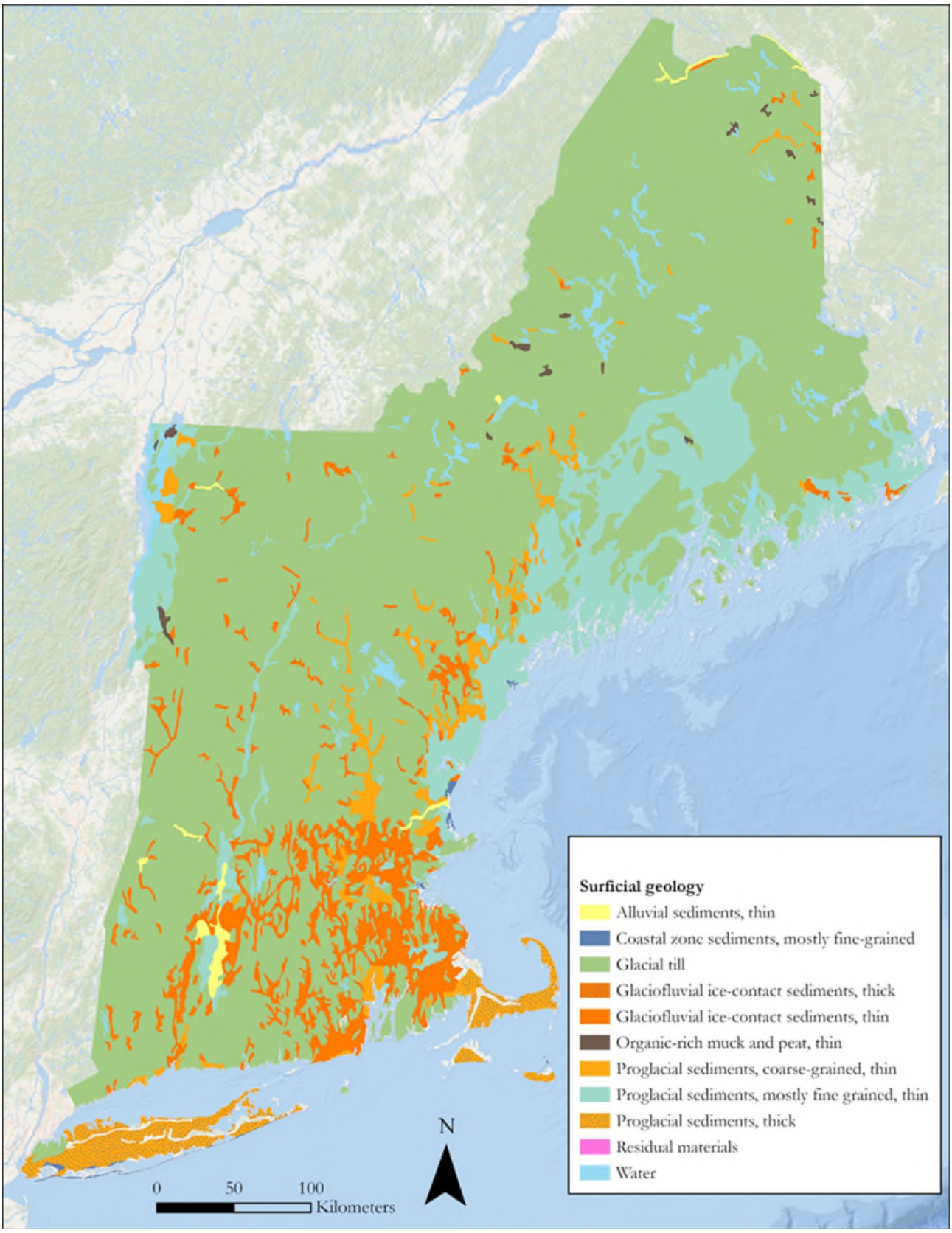

Figure 5. Merged geologies based on Table 4.

Kappa

Earthquake accelerograms were collected for 43 M3-M5.3 earthquakes that occurred within the Northeastern US and Southeastern Canada between 2005 and 2020 (Table A.1, appendix). Acceleration data were gathered from 67 different seismic stations belonging to one of the CN, IU, LD, N4, NE, or TA seismic networks (Table A.2, appendix). For each of the 67 stations, 2 horizontal component accelerograms were downloaded from the IRIS DMC for each of the 43 earthquakes for which data were available. Every accelerogram (Figure 6) that was downloaded was visually inspected to identify the S-wave first arrival, and the accelerogram was windowed to include 3 minutes of data after the selected S-wave first arrival time. If an accelerogram did not contain a visible S-wave first arrival, it was removed from the processing. Once an accelerogram was windowed to 3 minutes of data (Figure 6), it was then put through a Fourier Transform to produce a plot of the logarithm of the acceleration spectra versus frequency (Figure 7). Each acceleration spectra plot was then examined visually to determine an edge frequency (f_e) and a maximum frequency (f_{max}) between which the decay in the logarithm of the acceleration spectra with increasing frequency could be approximated as linear (Figure 7). A linear regression was then performed on the logarithm of the acceleration spectra between f_e and f_{max}, and κ was calculated as the slope of that linear regression. κ values were found for both horizontal acceleration components for each of the 43 earthquakes at each of the 67 seismic stations where data were available, and S-wave first arrivals could be determined through visual inspection.

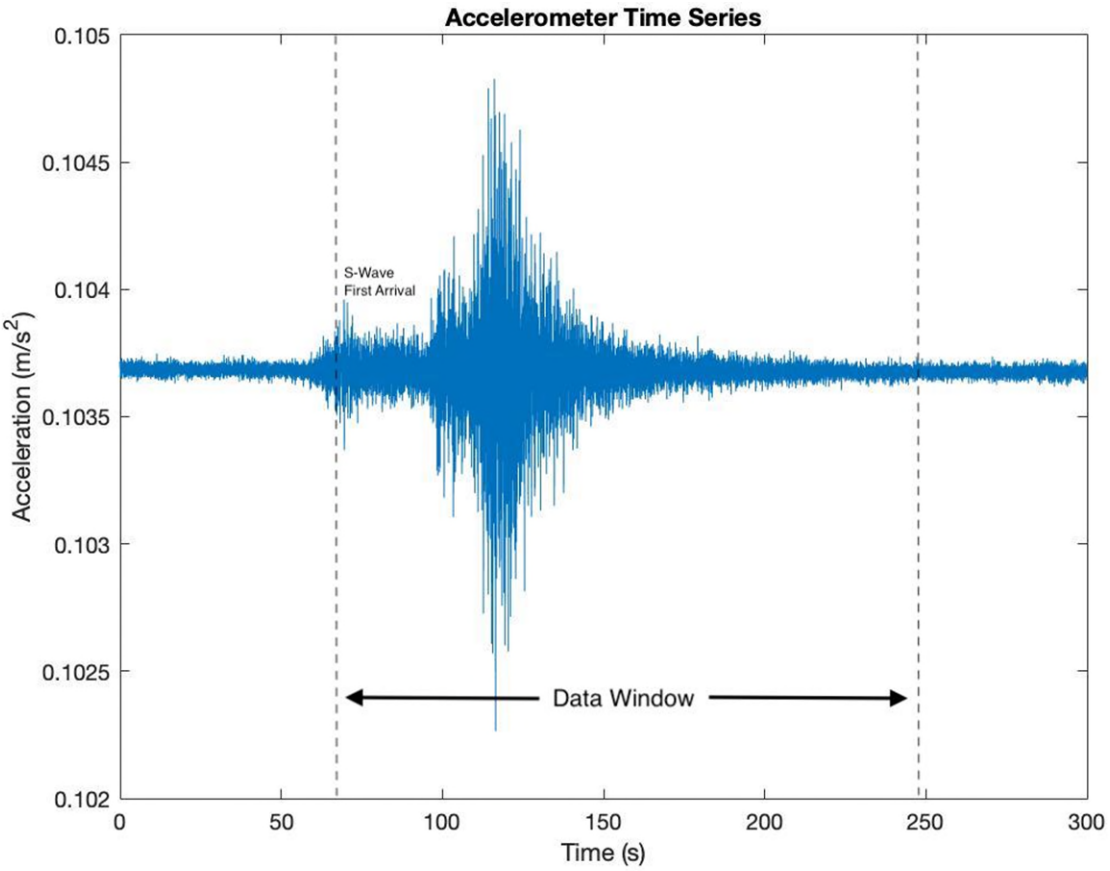

Figure 6. Sample acceleration data versus time. The S-wave first arrival is indicated by the leftmost vertical dashed line. The rightmost vertical dashed line indicates the end of the data window that includes 3 minutes of acceleration data starting from the S-wave first arrival. A κ value was determined from the amplitude spectrum of the data in the time window.

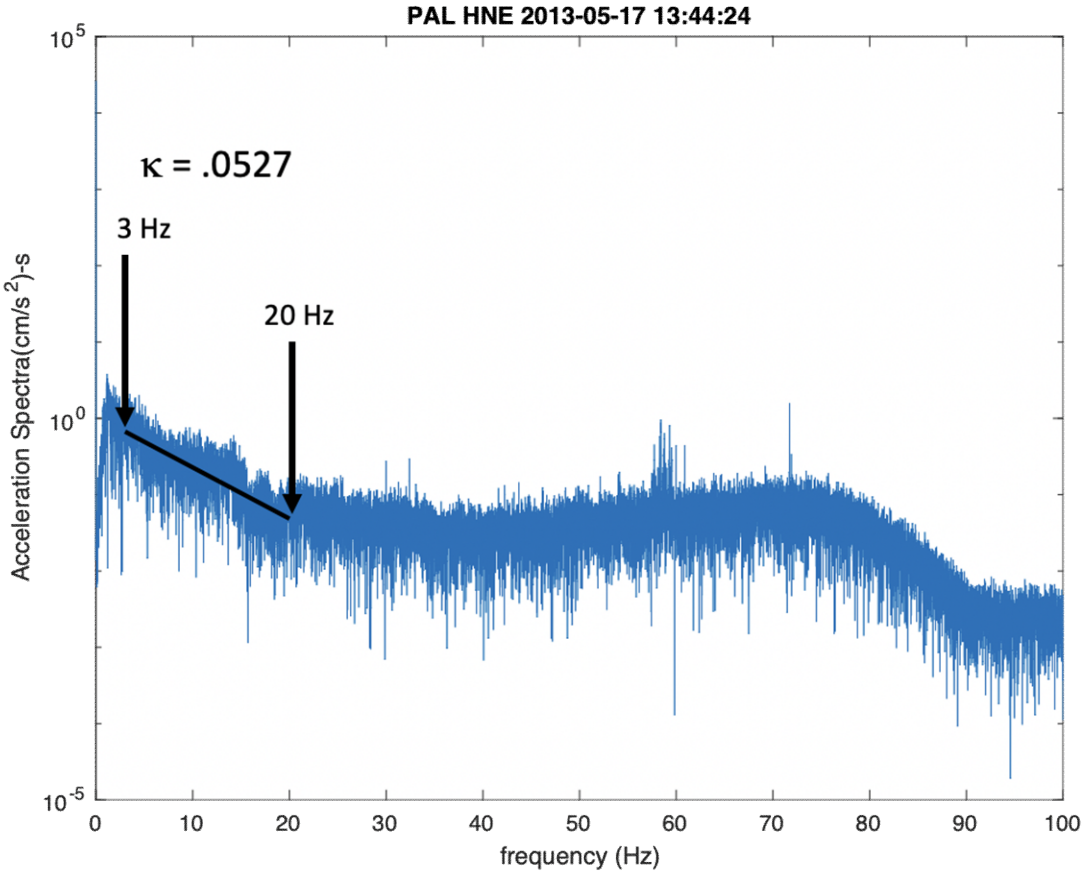

Figure 7. A semilogarithmic plot of the acceleration spectrum versus frequency of the E-W accelerogram from station PAL of an earthquake recorded in 2013. The edge frequency f_e and maximum frequency f_{max} were selected by visual inspection as 5 and 20 Hz, respectively. Plotted atop the acceleration spectrum is the linear regression of the spectra between f_e and f_{max}. The slope of this regression is used as the value of κ for this earthquake recording.

For each of the two horizontal components for each of the 67 stations that had at least two κ values calculated, a κ_0 value (the value of κ if the distance between the earthquake and the station was 0 km) was also calculated (Table A.2, Appendix). κ_0 for a seismic station location was calculated from the y-intercept of the linear regression of the κ values versus epicentral distance for the data from that seismic station (Figure 8). Each horizontal component of each of the 67 stations had a κ_0 calculated (Table A.2).

(a)

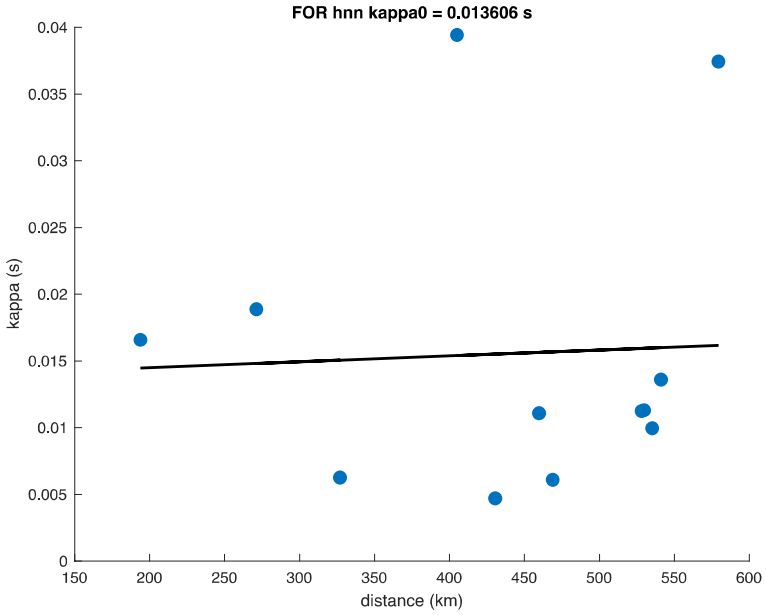

(b)

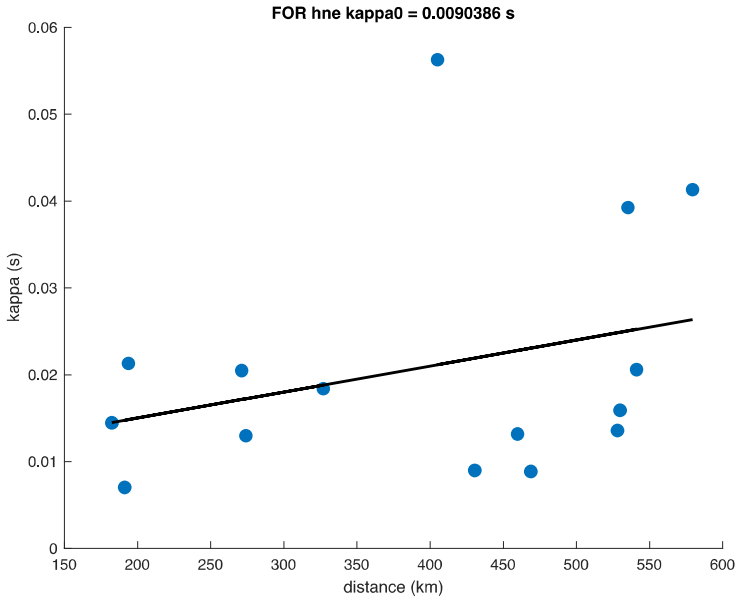

Figure 8. A scatter plot of all values of κ calculated using different earthquakes for (a) the N-S component and (b) the E-W component of ground motions at station FOR in New York City. A linear regression was performed on the values of κ and the distance values in each of these two plots, with each intercept value yielding κ_0 for that ground-motion component. The two independent determinations of κ_0 at this station are close in value to each other.

Results

f_0 distributions

After performing the spatial join of the f_0 distributions with the regrouped surficial geology units described above, we get 8 distibutions of f_0 with glacial till having the highest f_0 median and thick proglacial sediments having the lowest f_0 median as shown in Figure 9. The resulting map is shown in Figure 10a with boxplots for each surficial unit in Figure 10b. The thickest surficial units from Figure 4 also have the lowest f_0 values (Figure 10b). These are located on Cape Cod and Long Island, both of which are unconsolidated thick terminal moraines. Within the Connecticut River Valley there is a band of low-frequency thin alluvial sediments (median 2.13 Hz) adjacent to a band of proglacial sediments, mostly fine-grained, thin (median 3.26 Hz). The alluvial sediments in this structure are comprised of the flood-plain alluvium deposited by the Connecticut River, and they sit on fine grained clays of Glacial Lake Hitchcock. Adjacent to Lake Champlain in Vermont is a large patch of thin proglacial sediments, mostly fine-grained, (median 3.26 Hz) which is composed of the Champlain Sea sediments, a marine clay deposited when Lake Champlain was existed during the last glaciation period. Along the east coast of New England, particularly in the Boston Basin and Maine, is a band of fine coastal zone sediments. These are the Boston Blue Clay and the Presumpscot formation and, like the Champlain Sea sediments, are marine clays deposited when relative sea level was higher than it is today. Figure 11 provides more detailed maps of these regions.

In our field work we noted that the Maine coast f_0 values tend to be highly variable with some deep pockets, but often shallow veneers of overburden, and that the entire area of thin, mostly fine-grained proglacial sediments shown in the map in Figure 11a has higher f_0 values than the mapped median of 2.70 Hz. We could remedy this in future work by collecting additional data and further subdividing the surificial geologic units with local data. For example, in the same surficial geologic region, the Boston Basin is composed of Boston Blue Clay which on the Conterminous map is mapped as thin mostly fine-grained proglacial sediments and coastal zone sediments has f_0 medians of 2.70 and 3.30 Hz respectively. Similarly, many of the river valleys that are smaller than the Connecticut River Valley with less sediment build-up in their river beds have a median f_0 of 4 Hz, indicating thin unconsolidated sediments. Finally, in the vast majority of the land area in New England, the f_0 median is 6.16 Hz, indicating high velocities and thin overburdem fast tills and thus high f_0 values.

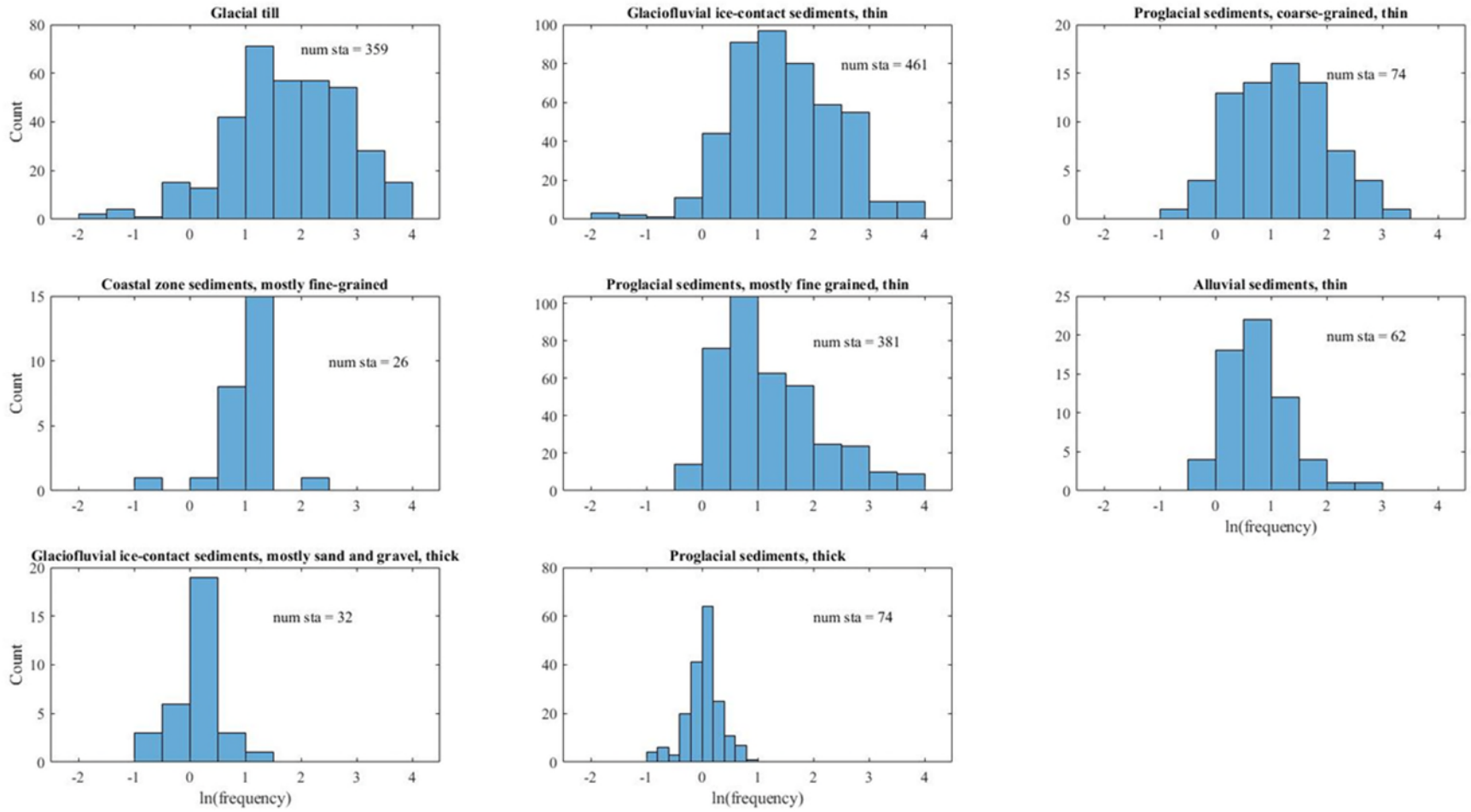

Figure 9. Histograms of the f_0 distributions within each surifical geologic unit

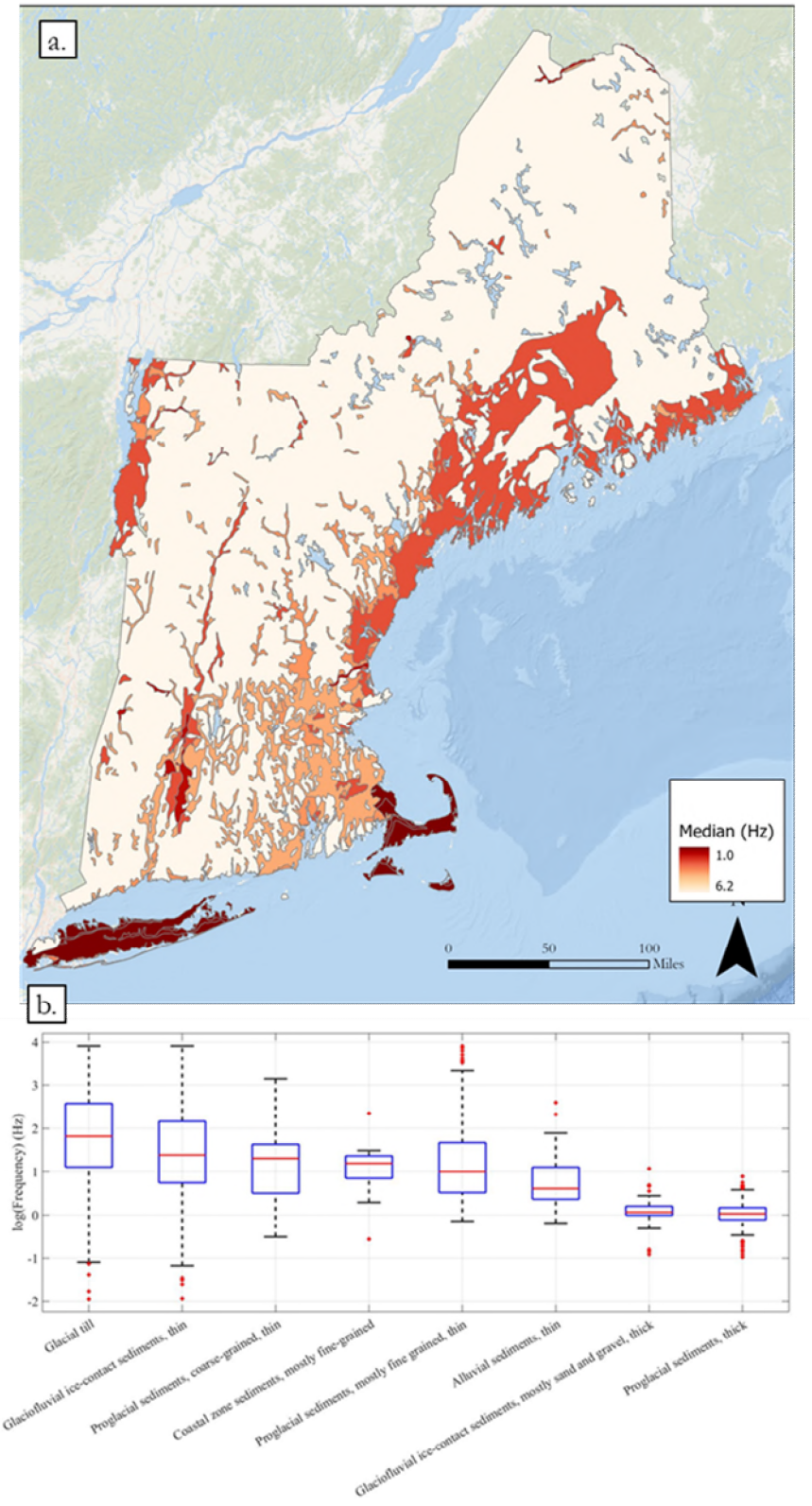

Figure 10. Results of the spatial join of the f_0 stations with each of the surficial geologic units from Table 4. a) A map of the medians of the f_0 distribution of each unit, these medians are also in Table 5. b) A box and whisker plot of all the f_0 distributions in each surficial unit

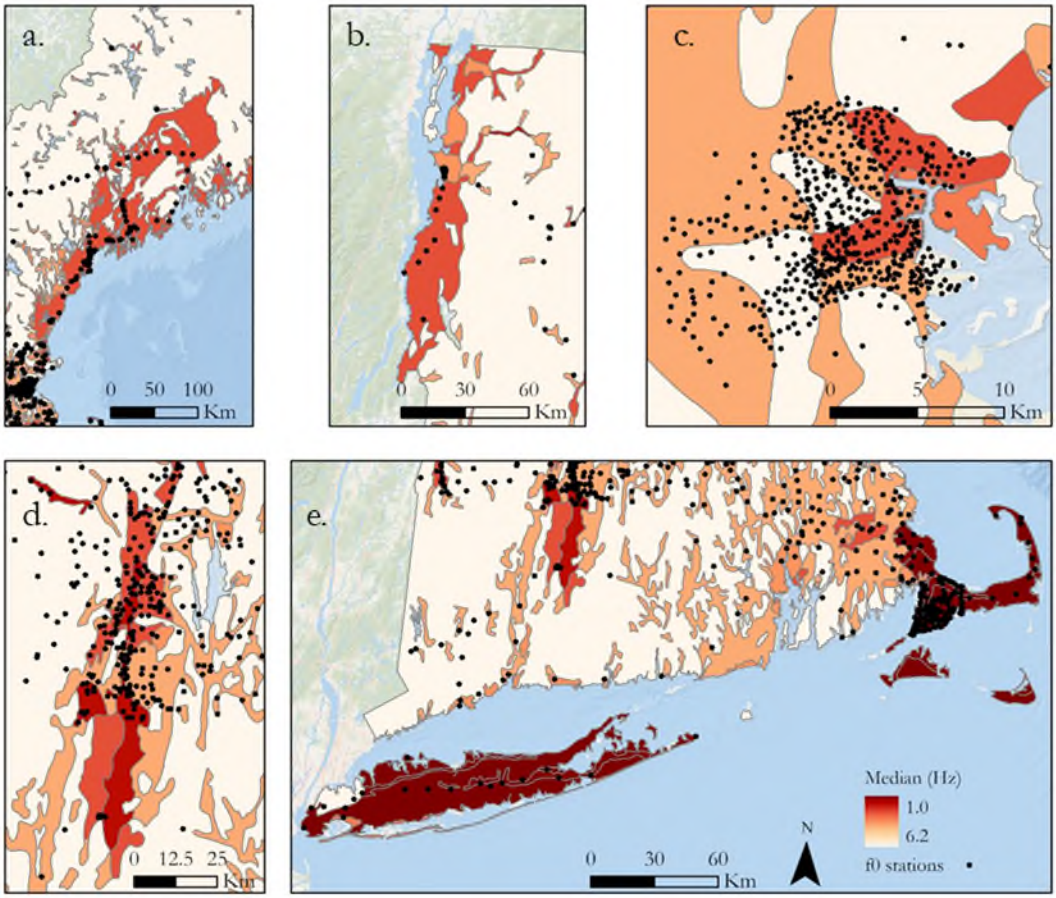

Figure 11. Zoomed in major geologic units in Figure 11 a) the Maine coast, b) the Lake Champlain coast, c) the Connecticut River Valley, d) Cape Cod and Long Island. The f_0 station locations are plotted in black.

There are five significant regions that stand out in this study: the Maine coast, the Lake Champlain coast, the Boston Basin, the Connecticut River Valley and Cape Cod and Long Island. The Maine coast is classified in the Conterminous map as thin, mostly fine-grained proglacial sediments (Figure 11a). This unit is known as the "Presumpscot formation" and was deposited when relative sea level was higher than it is today during the Wisconsin glacial period. In the current map (Figure 11a), the Maine coast f_0 median is represented by a surficial geologic unit (thin, fine-grained proglacial sediment) which has a median of 2.7 Hz. This value includes data from other areas in New England classified as thin, mostly fine-grained proglacial sediments. We observed that the thin, mostly fine-grained proglacial sediments in Maine tend to have higher f_0 values than this median. The Box and Whisker plot in Figure 10b has several outliers above 3.25 Hz in the thin, mostly fine-grained proglacial sediments distribution, the majority of which are found on the Maine Coast. In Figure 12, we have zoomed in on these stations, 80% (84/105) of which have f_0 values above the database's thin, fine-grained proglacial sediment f_0 median of 2.7 Hz. Many of the stastions with f_0 measurements below the median are located in Portland and south of Portland and are increasingly above the median to the north Portland. We note that the coast gets rockier to the north and thus the mapped clays are thinner, causing lower f_0 measurements. In future work, we plan to split the database up further by region in addition to geologic unit to account for these variations within a single geologic unit.

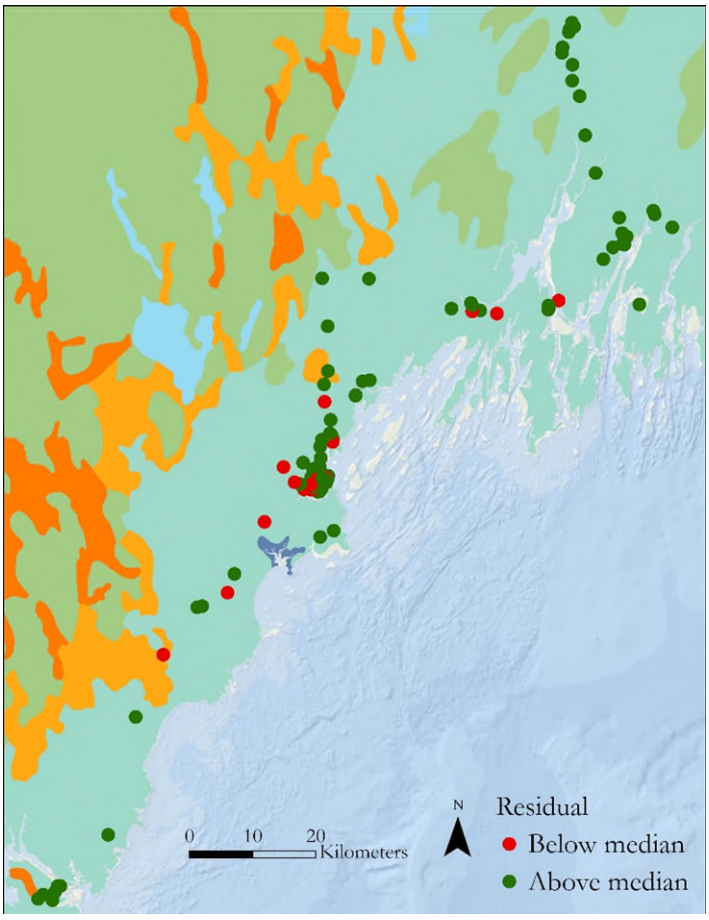

Figure 12. Maine coast f_0 residuals. Stations where the f_0 values are above the thin, fine-grained proglacial sediment f_0 median of 2.7 Hz are shown in green and where they are below are shown in red. The geologic color scheme is the same as Figure 5 and each unit's f_0 statistics and Vs_{avg} estimates are in Table 5.

The Coast of Lake Champlain is also composed of thin, mostly fine-grained proglacial sediments, a unit known as the Champlain Sea Sediments (Figure 11b). Like the Maine Coast, these sediments were deposited during the last glacial period. We found these sediments to be consistently lower frequency than the Maine coast with considerably fewer exposed rock outcroppings and topographic variation. Like the Maine and Lake Champlain coasts, the Boston Basin is also composed of thin, mostly fine-grained proglacial sediments (2.7 Hz f_0 median) also with coastal zone sediments (3.31 Hz f_0 median) (Figure 11c). These fine-grained sediments are the Boston Blue Clay and were extensively mapped in Yilar at al. (2017). The Connecticut River Valley (Figure 11d) is mapped as both thin, mostly fine-grained proglacial sediments and as alluvial sediments. The fine sediments are the clay deposits of Glacial Lake Hitchcock, and the alluvial sediments are deposited on the flood plain of the Connecticut River. Finally, Cape Cod and Long Island are entirely classified as thick glaciofluvial ice contact sediments and thick proglacial sediments, both of which have the lowest f_0 medians in the study at 1.06 and 1.03 Hz respectively (Figure 11e).

Kappa

Many of the 67 stations had no data for some of the 43 earthquakes of Table A.1 or the acceleration data that were available did not contain a clear S-wave first arrival, which made it impossible to window

those data in a manner that was consistent with the windowing at those stations with clear (or relatively clear) S-wave arrives. The result of these data limitations was that, on average, each of the horizontal components for each station only had 4 values of κ calculated from which a κ_0 could be found (Table A.2), and just 3 stations had more than 10 separate κ determinations from which κ_0 could be found. In some cases, a negative value of κ_0 was found. This is a result that is not physical but arose due to the scatter in the data masking the small positive values of κ_0 that should have been measured. At some stations, the value of κ_0 from one horizontal component of ground motion is positive whereas the other component has a negative value of κ_0.

Figures 13, 14 and 15 show maps of the values of k_0 as determined in this study. Figures 13 and 14 show the k_0 values for the N-S and E-W ground-motion components separately, and Figure 15 shows the average of the two κ_0 values for each station. All three maps show similar results for each station. κ_0 values are consistently less than 0.02 s throughout most of New England and New York, but reach higher values at a few isolated sites, such as values above 0.30 s near the St. Lawrence River northeast of Quebec City. The κ_0 values in New England and New York likely reflect that had bedrock is close to the surface at the locations of many of the regional seismic stations that were used in this study. It may also reflect that sites underlain by glacial till may have very small κ_0 values. The largest κ_0 values in these figures come from sites near major rivers, which probably indicates that those sites are at locations with local thick accumulations of river sediments. Such sites likely have lower f_0 values as well.

Figure 16 shows the mean κ_0 values from the two separate horizontal components for a site in northern New York, a site in east-central New York and several sites in the greater New York City area. This figure emphasizes the general pattern seen in Figures 13-15, namely that the κ_0 values in the region do not depend on whether the sites are close to the coastline or are located well inland where thicker glacial ice was experienced and thicker layers of glacial sediments were laid down.

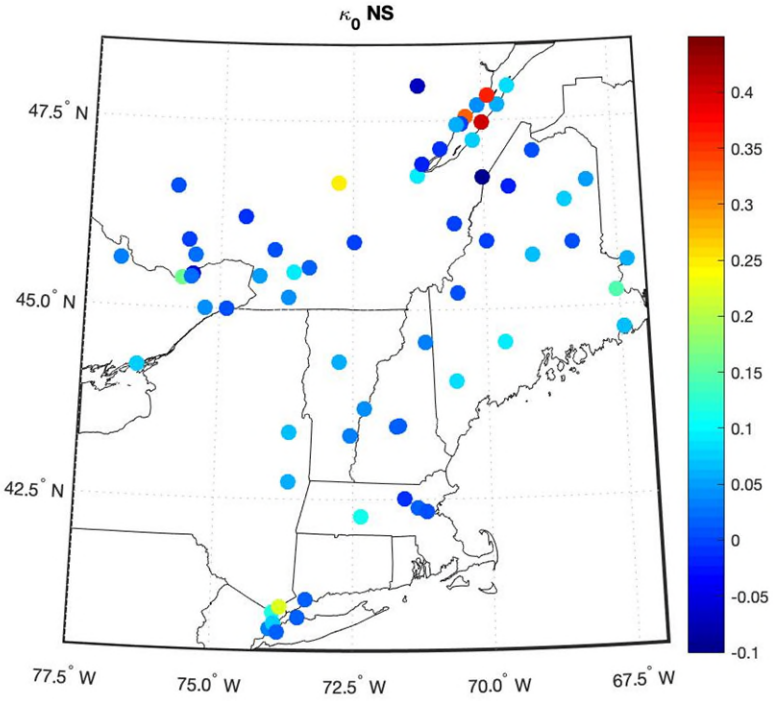

Figure 13. κ_0 values calculated for the North South components of each of the 67 seismic stations in the region of this study are displayed using the colorbar.

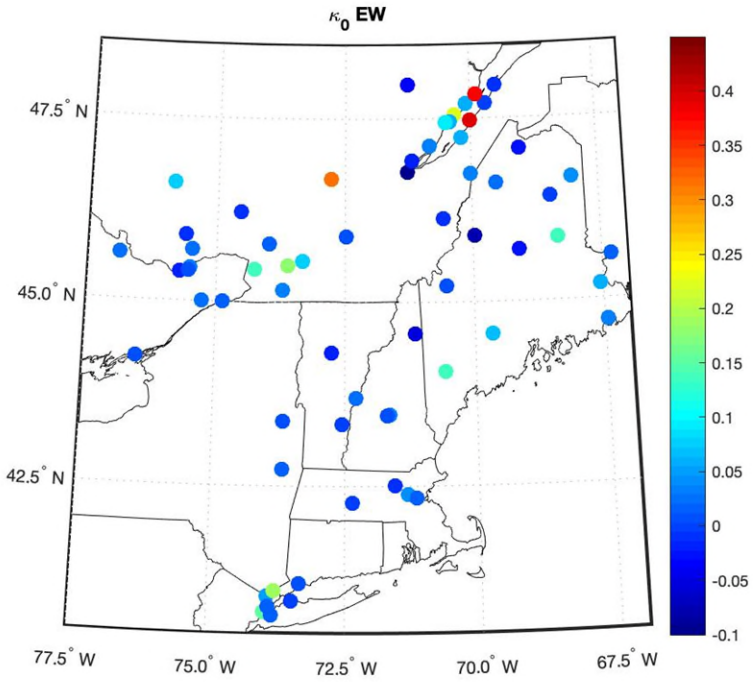

Figure 14. κ_0 values calculated for the East West components of each of the 67 seismic stations in the region of study are displayed using the colorbar.

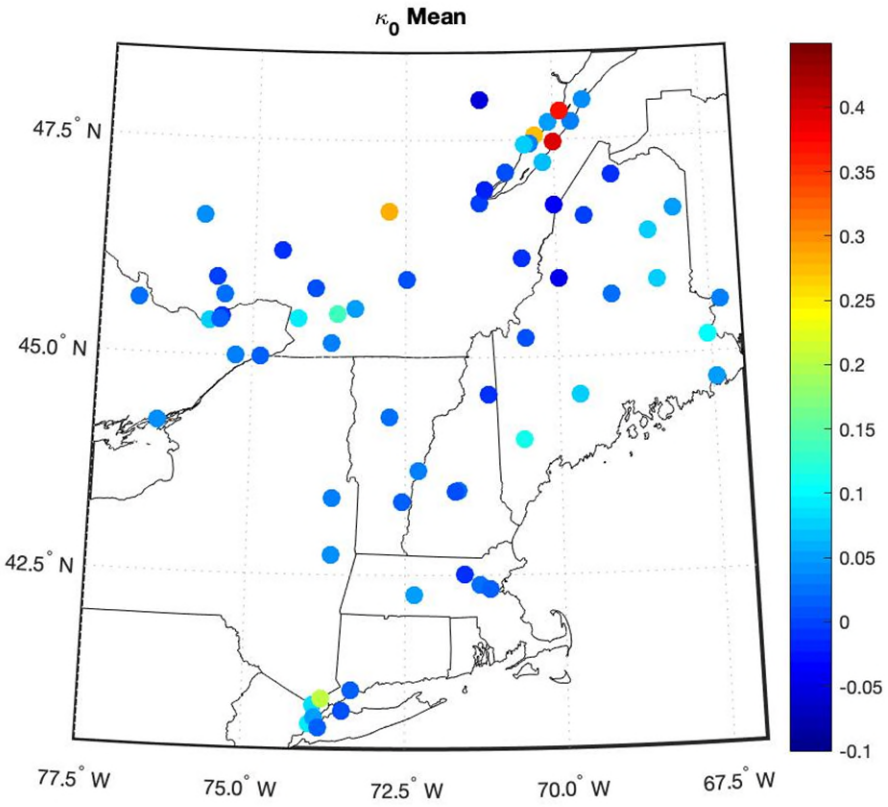

Figure 15. The mean of the North South and the East West component κ_0 values calculated for each of the 67 seismic stations in the region of study are displayed using the colorbar.

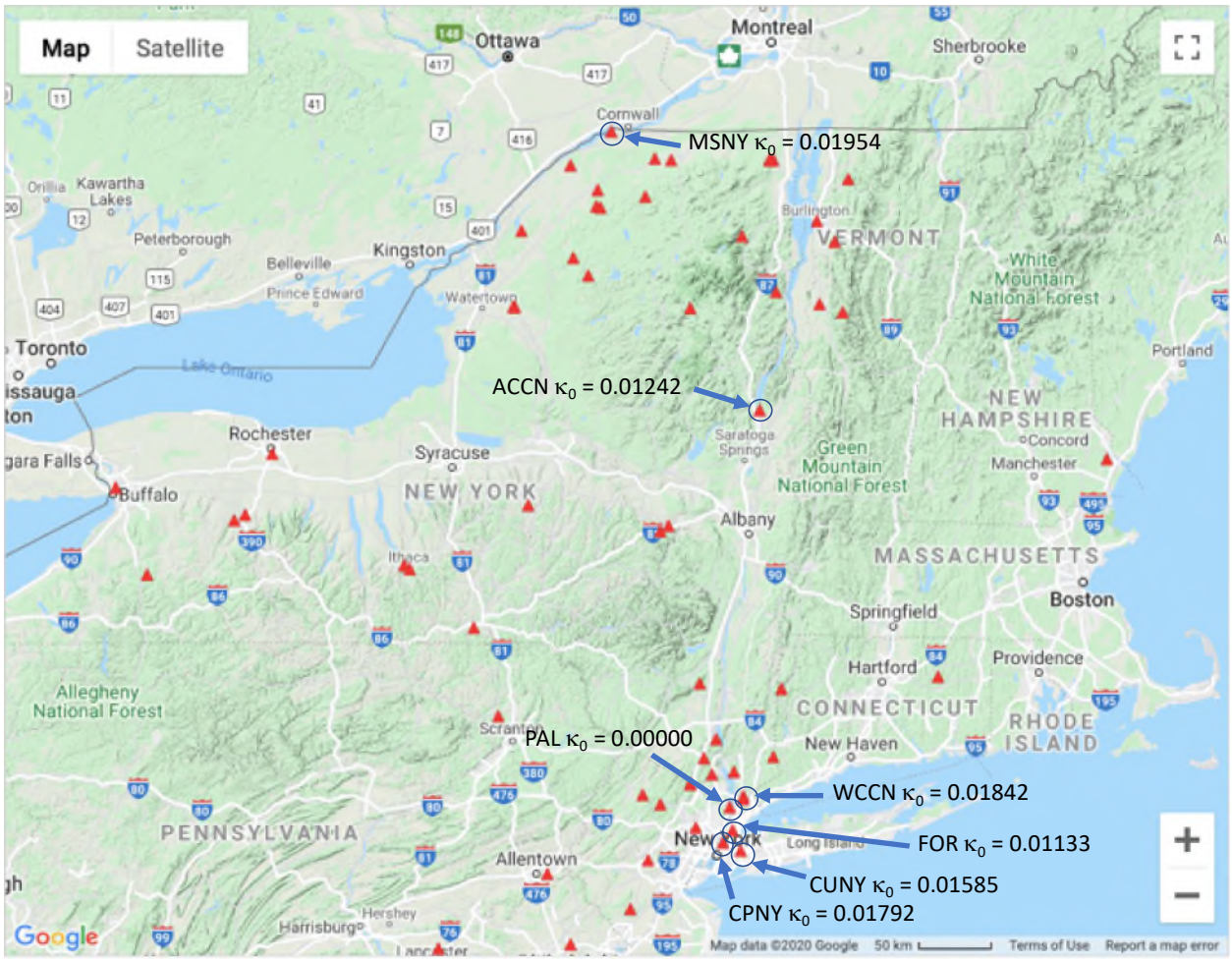

Figure 16. Map showing some k_0 values measured in northern New York, in eastern New York along the Hudson River and in the greater New York City area. These values were computed from the mean of the two k_0 values for each station.

Discussion

The f_0 measurement is useful because it incorporates information from both depth and shear wave velocity, both driving factors in a soil transfer function as described in equation 3

$$f_0 = \frac{V_s}{4d} \tag{3}$$

where V_s is the shear wave velocity of the overburden and d is the depth of the overburden. According to equation 3, when V_s decreases or d increases, f_0 decreases. A low f_0 value measured in the field, therefore, means that a soil deposit is either soft or deep or, most likely, some combination of the two. An additional benefit of the HVSR technique is that it is relatively easy compute and cheap to collect and thus one can obtain a significant number of measurements. For the analyses that we perform here, this is vital.

In this study we estimate Vs_{avg}, the average shear wave velocity of the overburden, for each of the eight surficial geologic units in Table 5 using several measured profiles in the region and expert judgement. We then calculate depth and *Vs30* using the relationship $f_0 = Vs_{avg}/4d$ with the f_0 and Vs_{avg} values in Table 5 and a bedrock shear wave velocity of 2500 m/s. Consider Figure 11d, the f_0 median map of the Connecticut River Valley. This map shows that the Valley is composed of alluvial sediments with a median frequency of 1.83 Hz and fine-grained proglacial sediments with median frequency 2.70 Hz. If we assume that the shear wave velocity profile across the Connecticut River Valley is a one-layer over half space model with a shear wave velocity in the thin alluvial sediments of 220 m/s (Table 5) with an f_0 value of 1.83 Hz, then a median depth estimate of the unit is approximately 30 meters. The *Vs30* estimate for this alluvial sediment in the Connecticut River Valley is 220 m/s and the *Vs30*-based site class is D. For the fine-grained proglacial sediments, assuming a shear wave velocity of 180 m/s and using the median f_0 value of 2.70 Hz, the median depth estimate is approximately 17 meters. In this profile, we need to account for the bottom 13 meters of bedrock on the *Vs30* calculation. The *Vs30* estimate for this unit is 301 m/s, still a site class D, but with a higher *Vs30* estimate than the alluvial sediments because of the shallow depth to bedrock. In this way, we can take the f_0 maps, assume an average shear wave velocity of the overburden using the surficial geologic classification, calculate the depth using equation 3 and make a prediction of the *Vs30*-based seismic site class (Figure 17). This methodology is also outlined in Hassani and Atkinson (2016) and plots of these relationships for our classified surficial geologic units in Table 5 are shown in Figure 17.

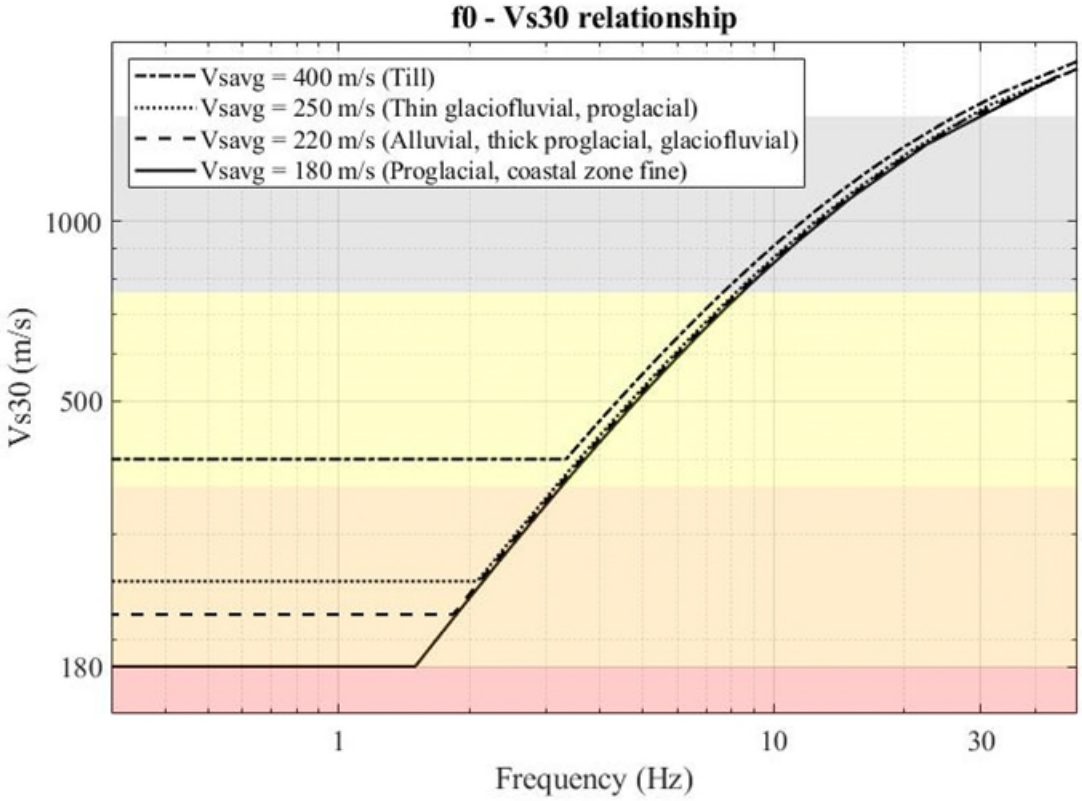

Figure 17. Relationship between f_0 and *Vs30* for the 8 average shear wave velocity estimates of important surficial units in the study. We use a single line to represent several units in some cases where units have similar velocities. The flat line in the low frequency ranges represents the point at which the overburden layer exceeds 30 meters and thus the *Vs30* value is equal to the average shear wave velocity of the overburden layer. A shear wave velocity of 2500 m/s was used for the basement layer in this plot. The example from the Connecticut river valley described above uses the dashed and solid lines in the figure. The background colors represent site classes, red is site class E, orange is D, yellow is C, grey is B, and white is A. This plot is modeled after Figure 6 in Hassani and Atkinson (2016).

Several previous studies have reported κ_0 values for sites in different parts of eastern North America. The results of those studies are summarized in Table 6 Although the range of κ_0 values found in this study is similar to the κ_0 ranges found in those previous studies, the average κ_0 value of this study is the highest of any average value reported in Table A.2. This may reflect that this study determined κ_0 values for all possible station sites in the northeastern U.S. and southeastern Canada whereas the previous studies generally focused their observations on rock sites. The large scatter in the κ data points from this study (e.g., Figure 14) may have also influenced the κ_0 results. Most of the earthquakes in this study (Table A.1) had magnitudes smaller than M4.0, which means that the signal-to-noise ratio of the events were small. The strong-ground motion recordings from the largest earthquakes in this data set were not analyzed separately because most stations had only 1 or 2 recordings from which κ_0 could be determined. It should be noted that a study of κ_0 values for hard-rock sites in France found κ_0 values around 0.02 s, somewhere between the κ_0 values reported by Atkinson (1996) for eastern North America and western North America. The somewhat higher average κ_0 value found in this study compared to those found in previous studies for eastern North America is probably not a significant difference when compared to the κ_0 values found in France.

One important reason why κ_0 values are important is that they are a necessary input into simulations of strong ground motions. Such simulations have been used by some investigators to derive ground-motion models based on the simulation (e.g., Boore, 2003; Yenier and Atkinson, 2015; and Atkinson, 2020). As ground-motion simulation methods become more reliable, better constraints on the κ_0 inputs will be needed to produce the most accurate range of possible ground motions.

Table 6. Summary of k_0 Determinations in Central and Eastern North America

Source	Mean k0 (s)	Range k0 (s)	Site Condition
Silva and Darragh (1995)	0.007	0.004-0.016	Hard rock
Silva and Darragh (1995)	0.007	0.004-0.016	Hard rock
Atkinson (1996)	0.002	0-0.004	Hard rock
Chapman et al. (2003)	0.009	0-0.018	Hard rock
Campbell (2003)	0.004	0.007	Hard rock
Atkinson and Boore (2006)	0.005	0-0.01	Hard rock
This study	0.01364	0-0.01954	Various

Conclusions

New England glaciated terrain consistently has high impedance contrasts due to high velocity bedrock and the soft, unconsolidated nature of many of the typical glaciated terrain deposits. We found that the f_0 measurement works well in New England and that when grouping the f_0 measurements by surficial geology, the large, unconsolidated surficial units display lower f_0 values than the typical till veneer in the rest of the region. Specifically, Cape Cod and Long Island have the lowest f_0 values in our study region, which we interpret as being the deepest thicknesses of sediments in the region, a statement that is consistent with the thickness classifications from the conterminous US surficial map. We also found that the marine clay sediments in the Boston Basin, the coast of Lake Champlain and the Maine coast tend to have low f_0 values. These units, however, have f_0 values that are very driven by depth to bedrock and therefore can vary widely in short distances. Finally, the river floodplain/glacial lake structure in the Connecticut River Valley also has low frequencies. Other glacial lakes and river floodplains in the region also have low f_0 values, but none on the scale of the Connecticut River Valley. Using Vs estimates for the sediments in each geologic unit, these regional f_0 maps can be used directly to create maps of *Vs30* and site class. Future work will subdivide some of the geologic units to allow for local variation in sediment properties and thickness.

This current study provides additional data on the values that are appropriate for the northeastern U.S. and southeastern Canada. We calculate κ_0 values for regional seismic stations on rock and sediment sites in New England. κ_0 values are consistently less than 0.02 s throughout most of New England and New York, reaching above 0.30 s near the St. Lawrence River northeast of Quebec City.

References

Anderson, J.G., and S.E. Hough (1984). A model for the shape of the Fourier amplitude spectrum of acceleration at high frequencies, *Bull. Seism. Soc. Am.* **74**, 1969-1993.

Atkinson, G.M. (1996). The high-frequency shape of the source spectrum for earthquakes in eastern and western Canada, *Bull. Seism. Soc. Am.* **86**, 106-112.

Atkinson, G.M. (2004). Empirical attenuation of ground-motion spectral amplitudes in southeastern Canada and the Northeastern United States, *Bull. Seism. Soc. Am.* **94**, 1079-1095.

Atkinson, G.M. (2020). The interface between empirical and simulation-based ground-motion models, *PAGEOPH* **177**, 2069-2081, doi: 10.1007/s00024-18-2044-1.

Atkinson, G.M., and D.M. Boore (2006). Earthquake ground-motion prediction equations for eastern North America, *Bull. Seism. Soc. Am.* **96**, 2181-2205, doi: 10.1785/0120050245.

Baise, L. G., Kaklamanos, J., Berry, B.M., Thompson, E.M. (2016). Soil Amplification with a strong impedance contrast: Boston Massachusetts. *Engineering Geology* 202 (2016) 1-13.

Boore, D.M. (2003). Simulation of ground motion using the stochastic method, *PAGEOPH* **160**, 635-676.

Braganza, S., Atkinson, G.M., Ghofrani, H., Hassani, B., Chouinard, L., Rosset, P., Motazedian, D., Hunter, J; Modeling Site Amplification in Eastern Canada on a Regional Scale. *Seismological Research Letters* 2016;; 87 (4): 1008–1021. doi: https://doi.org/10.1785/0220160009

Campbell K.W. (2009). Estimates of shear-wave Q and κ_0 for unconsolidated and semiconsolidated sediments in Eastern North America, *Bull. Seism. Soc. Am.* **99**, 2365-2392, doi: 101785/0210080116.

Carpenter, N.S., Wang, Z., Woolery, E.W., Rong, M (2018) Estimating Site Response with Recordings from Deep Boreholes and HVSR: Examples from the Mississippi Embayment of the Central United States. Bulletin of the Seismological Society of America 2018; 108 (3A): 1199–1209. doi: https://doi.org/10.1785/0120170156

Chandler, A.M., N.T.K. Lam and H.H. Tsang (2006). Near-surface attenuation modelling based on rock shear-wave velocity profile, *Soil Dynamics and Earthquake Engineering* **26**, 1004-1014.

Chapman, M.C., P. Talwani and R.C. Cannon (2003). Ground-motion attenuation in the Atlantic coastal plain near Charleston, South Carolina, *Bull. Seism. Soc. Am.* **93**, 998-1011.

Chuanbin Zhu, Fabrice Cotton, Marco Pilz; Detecting Site Resonant Frequency Using HVSR: Fourier versus Response Spectrum and the First versus the Highest Peak Frequency. *Bulletin of the Seismological Society of America* 2020;; 110 (2): 427–440. doi: https://doi.org/10.1785/0120190186

Douglas, J., P. Gehl, L.F. Bonilla and C. Gelis (2010). A κ model for mainland France, *PAGEOPH* **167**, 1303-1315, doi: 10.1007/s00024-010-0146-5.

Fairchild, G.M., Lane, J.W., Jr., Voytek, E.B., and LeBlanc, D.R., 2013, Bedrock topography of western Cape Cod, Massachusetts, based on bedrock altitudes from geologic borings and analysis of ambient seismic noise by the horizontal-to-vertical spectral-ratio method: *U.S. Geological Survey Scientific Investigations Map 3233*.

Gallipoli, M.R., Mucciarelli, M (2009) Comparison of Site Classification from VS_{30}, VS_{10}, and HVSR in Italy. *Bulletin of the Seismological Society of America* 2009; 99 (1): 340–351. doi: https://doi.org/10.1785/0120080083

Hassani, B., Atkinson, G.M. (2016) Applicability of the Site Fundamental Frequency as a VS_{30} Proxy for Central and Eastern North America. *Bulletin of the Seismological Society of America* 2016; 106 (2): 653–664. doi: https://doi.org/10.1785/0120150259

Hassani, B., and G.M. Atkinson (2018). Adjustable generic ground-motion prediction equation based on equivalent point-source simulations: accounting for kappa effects, *Bull. Seism. Soc. Am.* **108**, 913-928, doi: 10.1785/0120170333.

Kyriazis Pitilakis, et al., Soil Dynamics and Earthquake Engineering, https://doi.org/10.1016/j.soildyn.2018.03.030

Laurendeau, A., F. Cotton, O.-J. Ktenidou, L.-F. Bonilla and F. Hollender (2013). Rock and stiff-soil site amplification: Dependency on V_{S30} and kappa (κ_0), *Bull. Seism. Soc. Am.* **103**, 3131-3148, doi: 10.1785/0120130020.

Lermo J. Chávez-Garcia F. J. (1993). Site effects evaluation using spectral ratios with only one station, *Bull. Seismol. Soc. Am.* 84, 1350–1364.

Nakamura, Y. (1989) A Method for Dynamic Characteristics Estimation of Subsurface using Microtremor on the Ground Surface. *Railway Technical Research Institute* 30(1): 25-33.

SESAME (2004a). Guidelines for the implementation of the H/V spectral ratio technique on ambient vibrations. European Commission - Research General Directorate.

SESAME (2004b). Site Effects Assessment Using Ambient Excitations. European Commission - Research General Directorate. Project No. EVG1-CT-2000-00026 SESAME.

Silva, W. and R. Darragh (1995). Engineering characterization of strong ground motion recorded at rock sites, *EPRI Report TR-102261*, 426 pp.

Soller, D.R., Reheis, M.C., Garrity, C.P., and Van Sistine, D.R., 2009, Map database for surficial materials in the conterminous United States: U.S. Geological Survey Data Series 425, scale 1:5,000,000 [https://pubs.usgs.gov/ds/425/].

Soller, D.R., and Reheis, M.C., compilers, 2004, Surficial materials in the conterminous United States: *U.S. Geological Survey Open-file Report 03-275*, scale 1:5,000,000

Thompson EM, Baise LG, Tanaka K, Kayen RE. (2012) A taxonomy of site response complexity. *Soil Dynamics and Earthquake Engineering*. 41(2012): 32-43.

Thompson, E.M., Carkin, B., Baise, L.G., and Kayen, R.E., 2014, Surface wave site characterization at 27 locations near Boston, Massachusetts, including 2 strong-motion stations: *U.S. Geological Survey Open-File Report 2014–1232*, 27 p., http://dx.doi.org/10.3133/ofr20141232

Van Houtte, C., S. Drouet and F. Cotton (2011). Analysis of the origins of κ (kappa) to compute hard rock to rock adjustment factors for GMPEs, *Bull. Seism. Soc. Am.* **101**, 2926-2941, doi: 10.1785/0120100345.

Wills, C. J., and K. B. Clahan (2006). Developing a map of geologically defined site-conditions categories for California, *Bull. Seism. Soc. Am.* 96, 1483–1501.

Yenier, E., and G.M. Atkinson (2015). Regionally adjustable generic ground-motion prediction equations based on equivalent point-source simulations: Application to central and eastern North America, *Bull. Seism. Soc. Am.* **105**, 1989-2009, doi: 10.1785/0120140322.

Yilar, E., Baise, L.G., Ebel, J.E. (2017) Using H/V measurements to determine depth to bedrock and Vs30 in Boston, Massachusetts. *Engineering Geology* 217, 12-22

Appendix

Table A.1 Each of the 43 M3-M5.3 earthquakes that occurred within the study region between 2005 and 2020.

3/6/2005	1:17:49	47.75	69.75	0.02	5.3
6/23/2010	17:41:43	45.87	75.49	19.26	4.9
5/17/2013	13:43:24	45.75	76.34	13	4.7
10/16/2012	23:12:24	43.6	70.65	3.6	4.5
10/3/2006	0:07:38	44.35	68.15	10.83	4.2
10/3/2006	0:07:38	44.35	68.15	2	4.2
11/15/2008	10:52:55	47.63	69.73	3.17	4.2
2/25/2006	1:39:23	45.66	75.23	13.8	4
10/10/2012	4:19:30	45.7	73.26	12.34	4
1/9/2006	15:35:41	45.07	73.91	15.67	3.9
5/9/2020	19:04:18	47.08	75.77	0.02	3.9
7/14/2006	9:34:49	46.92	68.68	23.87	3.8
9/18/2011	19:19:14	45.57	75.22	1.82	3.8
11/6/2012	9:05:29	45.59	74.62	17.86	3.8
12/12/2012	17:46:06	47.79	70.06	7.91	3.8
4/7/2006	8:31:42	47.38	70.46	22.59	3.7
7/23/2010	17:24:22	46.51	71.62	12.19	3.7
3/16/2011	17:36:57	45.58	74.55	6.44	3.7
7/15/2015	22:00:20	45.44	74.52	6.33	3.7
12/28/2017	8:51:07	47.54	76.9	5	3.7
10/1/2007	16:42:10	47.03	76.84	19.14	3.6
2/28/2010	3:51:25	45.75	74.5	5	3.6
5/17/2013	13:53:56	45.75	76.34	15.75	3.6
1/13/2020	10:38:00	44.99	73.96	3.47	3.6
9/25/2005	3:08:58	45.04	67.28	0.38	3.5
6/1/2006	9:34:27	46.62	67.44	15.33	3.5
7/11/2013	20:16:07	47.84	70.09	10.07	3.5
11/28/2015	5:16:53	45.01	74.87	0.02	3.5
3/13/2018	20:43:30	47.78	68.11	3.66	3.5
7/13/2019	17:56:50	47.05	76.35	19.44	3.5
9/22/2006	10:39:21	44.35	68.19	6.99	3.4
8/24/2011	17:14:33	44.71	74.39	0.02	3.3
12/4/2017	5:56:53	44.43	76.42	5	3.3
3/11/2020	10:43:40	43.29	73.64	10.4	3.3
12/29/2006	21:21:11	44.35	68.17	8.45	3.1

9/26/2010	3:28:10	43.29	71.66	3.4	3.1
1/12/2015	11:36:39	41.76	71.9	0.68	3.1
7/27/2019	0:17:16	44.62	74.45	2.03	3.1
12/13/2009	22:00:51	42.57	74.11	1.8	3
3/30/2010	20:42:19	44.67	68.75	4.35	3
6/3/2010	12:25:04	40.09	76.96	6.11	3
6/21/2013	10:14:28	44.52	69.75	10.37	3
9/27/2015	3:16:23	42.45	74.42	6.63	3

Table A.2 Each of the 67 different stations within the region and the κ_0 value calculated for each of the two horizontal components as well as the number of κ values that were calculated for each component and therefore used to calculate the value of κ_0.

Network	Station	Channel	Latitude	Longitude	Sample Rate (Hz)	κ_0	Slope (κ /km)	Number of κ Values
CN	A11	hnn	47.24	-70.2	100	7.21E-02	-9.03E-05	5
CN	A11	hne	47.24	-70.2	100	5.79E-02	-4.04E-05	5
CN	A16	hnn	47.47	-70.01	100	4.02E-01	-7.86E-04	5
CN	A16	hne	47.47	-70.01	100	3.94E-01	-7.83E-04	5
CN	A21	hnn	47.7	-69.69	100	6.00E-02	-2.91E-05	4
CN	A21	hne	47.7	-69.69	100	2.89E-03	8.26E-05	4
CN	A54	hnn	47.46	-70.41	100	-4.30E-03	8.97E-05	4
CN	A54	hne	47.46	-70.41	100	6.28E-02	-9.49E-05	4
CN	A61	hnn	47.69	-70.09	100	4.36E-02	-5.60E-05	4
CN	A61	hne	47.69	-70.09	100	6.10E-02	-8.56E-05	4
CN	A64	hnn	47.83	-69.89	100	3.57E-01	-6.74E-04	5
CN	A64	hne	47.83	-69.89	100	3.78E-01	-7.49E-04	5
CN	BCLQ	hnn	46.93	-71.17	100	-2.07E-02	7.48E-05	2
CN	BCLQ	hne	46.93	-71.17	100	-1.46E-02	9.14E-05	2
CN	BSPQ	hnn	47.44	-70.51	100	6.22E-02	-7.82E-05	3
CN	BSPQ	hne	47.44	-70.51	100	9.42E-02	-1.23E-04	3
CN	CACQ	hnn	47.95	-69.5	100	8.55E-02	-1.15E-04	3
CN	CACQ	hne	47.95	-69.5	100	-8.39E-03	6.91E-05	3
CN	COBO	hnn	45.63	-76.88	100	3.51E-02	-7.87E-05	2
CN	COBO	hne	45.63	-76.88	100	2.07E-02	-2.18E-05	2
CN	DPQ	hnn	46.68	-72.78	100	2.45E-01	-5.43E-04	6
CN	DPQ	hne	46.68	-72.78	100	3.20E-01	-6.91E-04	6
CN	DRMQ	hnn	45.9	-72.47	100	1.88E-03	7.79E-05	2
CN	DRMQ	hne	45.9	-72.47	100	5.79E-03	7.63E-05	3
CN	GAC	hnn	45.7	-75.48	100	2.60E-02	3.08E-05	5
CN	GAC	hne	45.7	-75.48	100	2.42E-02	4.73E-05	5

CN	GRQ	hnn	46.61	-75.86	100	6.28E-03	3.15E-05	5
CN	GRQ	hne	46.61	-75.86	100	8.04E-02	-1.76E-04	5
CN	KGNO	hnn	44.23	-76.49	100	7.65E-02	-1.82E-04	6
CN	KGNO	hne	44.23	-76.49	100	8.00E-03	6.61E-05	6
CN	LDAQ	hnn	47.96	-71.24	100	-6.90E-02	2.17E-04	4
CN	LDAQ	hne	47.96	-71.24	100	-3.34E-02	1.14E-04	4
CN	LMQ	hnn	47.55	-70.33	100	3.24E-01	-2.49E-04	5
CN	LMQ	hne	47.55	-70.33	100	2.24E-01	-2.86E-05	5
CN	MCNB	hnn	45.6	-67.32	100	5.69E-02	-7.02E-05	2
CN	MCNB	hne	45.6	-67.32	100	1.64E-02	-1.03E-05	2
CN	MNTQ	hnn	45.5	-73.62	100	9.71E-02	-2.23E-04	6
CN	MNTQ	hne	45.5	-73.62	100	1.78E-01	-4.43E-04	6
CN	MRBQ	hnn	45.8	-73.99	100	4.97E-03	-5.85E-06	3
CN	MRBQ	hne	45.8	-73.99	100	1.64E-02	-3.72E-05	3
CN	ORIO	hnn	45.45	-75.51	100	-5.09E-02	4.42E-04	6
CN	ORIO	hne	45.45	-75.51	100	3.25E-02	2.14E-04	7
CN	OTAO	hnn	45.41	-75.55	100	2.60E-02	6.56E-05	3
CN	OTAO	hne	45.41	-75.55	100	7.57E-03	1.25E-04	3
CN	OTT	hnn	45.39	-75.72	100	1.62E-01	-6.01E-05	4
CN	OTT	hne	45.39	-75.72	100	-1.51E-02	5.61E-04	4
CN	QCQ	hnn	46.78	-71.28	100	9.03E-02	-1.81E-04	3
CN	QCQ	hne	46.78	-71.28	100	-9.62E-02	3.99E-04	3
CN	RIGQ	hnn	45.45	-74.26	100	5.43E-02	-1.91E-04	3
CN	RIGQ	hne	45.45	-74.26	100	1.35E-01	-5.38E-04	3
CN	SFA	hnn	47.12	-70.83	100	-6.23E-03	8.70E-05	5
CN	SFA	hne	47.12	-70.83	100	2.97E-02	-5.69E-06	5
CN	SGRQ	hnn	46.14	-70.58	100	-1.36E-03	4.41E-05	2
CN	SGRQ	hne	46.14	-70.58	100	-9.80E-03	6.11E-05	2
CN	SJUQ	hnn	45.56	-73.32	100	1.90E-02	-3.08E-05	3
CN	SJUQ	hne	45.56	-73.32	100	7.52E-02	-2.47E-04	3
CN	SURQ	hnn	45.17	-73.71	100	3.88E-02	-6.41E-05	3
CN	SURQ	hne	45.17	-73.71	100	3.26E-02	-3.36E-05	3
CN	TRQ	hnn	46.22	-74.55	100	-5.48E-03	9.37E-05	6
CN	TRQ	hne	46.22	-74.55	100	-6.02E-03	1.14E-04	6
CN	VABQ	hnn	45.9	-75.61	100	8.33E-04	3.36E-04	12
CN	VABQ	hne	45.9	-75.61	100	-7.52E-03	1.98E-04	12
CN	WBO	hnn	45	-75.28	100	3.89E-02	-1.05E-04	7
CN	WBO	hne	45	-75.28	100	2.79E-02	-4.23E-05	7
IU	HRV	hn1	42.51	-71.56	100	-1.24E-02	2.73E-04	3

IU	HRV	hn2	42.51	-71.56	100	-5.49E-03	2.11E-04	3
LD	ACCN	hnn	43.38	-73.67	100	6.92E-02	-8.83E-05	2
LD	ACCN	hne	43.38	-73.67	100	5.14E-03	1.77E-04	2
LD	CPNY	hnn	40.79	-73.96	100	3.63E-02	-1.93E-06	7
LD	CPNY	hne	40.79	-73.96	100	1.49E-01	-2.05E-04	5
LD	CUNY	hnn	40.73	-73.82	100	1.87E-02	-6.56E-06	2
LD	CUNY	hne	40.73	-73.82	100	1.66E-02	2.85E-04	5
LD	FOR	hnn	40.86	-73.89	100	7.69E-02	-5.51E-05	13
LD	FOR	hne	40.86	-73.89	100	1.88E-02	3.39E-05	15
LD	MSNY	hnn	45	-74.86	100	1.12E-02	5.04E-05	5
LD	MSNY	hne	45	-74.86	100	1.41E-02	3.51E-05	5
LD	PAL	hnn	41.01	-73.91	100	1.20E-01	-1.15E-04	13
LD	PAL	hne	41.01	-73.91	100	5.29E-02	-1.97E-05	16
LD	WCCN	hnn	41.07	-73.79	100	2.24E-01	-1.33E-04	4
LD	WCCN	hne	41.07	-73.79	100	1.90E-01	-2.71E-04	5
N4	D62A	hnn	47.08	-69.05	100	8.79E-03	2.89E-04	4
N4	D62A	hne	47.08	-69.05	100	-2.37E-02	3.78E-04	4
N4	E63A	hnn	46.42	-68.46	100	7.25E-02	-1.09E-04	2
N4	F62A	hnn	45.9	-69.97	100	-3.06E-03	9.52E-05	3
N4	F62A	hne	45.9	-69.97	100	-7.89E-02	3.52E-04	3
N4	F64A	hnn	45.86	-68.35	100	7.91E-03	5.51E-05	2
N4	F64A	hne	45.86	-68.35	100	1.40E-01	-2.18E-04	2
N4	G62A	hnn	45.22	-70.53	100	3.74E-03	5.80E-05	3
N4	G62A	hne	45.22	-70.53	100	1.11E-02	3.48E-05	3
N4	J61A	hnn	43.35	-72.55	100	3.00E-02	4.91E-05	2
N4	J61A	hne	43.35	-72.55	100	-3.91E-03	1.65E-04	2
N4	N62A	hnn	40.93	-73.47	100	1.83E-02	9.74E-06	3
N4	N62A	hne	40.93	-73.47	100	1.16E-03	5.65E-05	3
NE	BCX	bnh	42.33	-71.17	40	4.87E-03	6.35E-05	2
NE	BCX	bne	42.33	-71.17	40	1.92E-02	3.66E-05	3
NE	EMMW	bnn	44.71	-67.46	40	6.52E-02	-9.22E-05	4
NE	EMMW	bne	44.71	-67.46	40	3.66E-02	-4.46E-05	3
NE	FFD	bnn	43.47	-71.65	40	1.88E-02	7.67E-05	4
NE	FFD	bne	43.47	-71.65	40	3.01E-02	3.95E-05	4
NE	HNH	bnn	43.71	-72.29	40	3.91E-02	-8.66E-05	3
NE	HNH	bne	43.71	-72.29	40	2.51E-02	-3.80E-05	3
NE	NHFNK	hnn	43.47	-71.69	200	1.22E-02	1.17E-05	2
NE	NHFNK	hne	43.47	-71.69	200	4.54E-03	2.84E-05	2
NE	PQI	bnn	46.67	-68.02	40	5.18E-02	-6.39E-05	3
NE	PQI	bne	46.67	-68.02	40	4.28E-02	-5.23E-05	4

NE	QUA2	bnn	42.28	-72.35	40	1.09E-01	-2.45E-04	3
NE	QUA2	bne	42.28	-72.35	40	-3.53E-03	5.72E-05	3
NE	TRY	bnn	42.73	-73.67	40	6.14E-02	-9.87E-05	3
NE	TRY	bne	42.73	-73.67	40	1.48E-02	4.70E-05	3
NE	VT1	bnn	44.32	-72.75	40	6.24E-02	2.39E-04	4
NE	VT1	bne	44.32	-72.75	40	-2.17E-02	3.38E-04	4
NE	WES	bnn	42.38	-71.32	40	1.78E-02	-3.11E-06	3
NE	WES	bne	42.38	-71.32	40	3.98E-02	-4.72E-05	3
NE	WSPT	bnn	41.17	-73.33	40	1.33E-02	-1.16E-05	3
NE	WSPT	bne	41.17	-73.33	40	1.04E-02	4.70E-05	3
NE	WVL	bnn	44.56	-69.66	40	9.56E-02	-1.94E-04	4
NE	WVL	bne	44.56	-69.66	40	6.34E-02	-1.31E-04	4
TA	E62A	hnn	46.62	-69.52	100	-1.85E-02	6.57E-05	2
TA	E62A	hne	46.62	-69.52	100	2.38E-02	-3.54E-05	2
TA	E63A	hnn	46.42	-68.46	100	-1.00E-02	3.02E-05	2
TA	E63A	hne	46.42	-68.46	100	-4.92E-03	2.16E-05	2
TA	F62A	hnn	45.9	-69.97	100	3.96E-02	-6.84E-05	2
TA	F62A	hne	45.9	-69.97	100	1.65E-02	-1.95E-05	2
TA	F63A	hnn	45.7	-69.1	100	7.15E-02	-8.55E-05	2
TA	F63A	hne	45.7	-69.1	100	-2.72E-02	1.22E-04	2
TA	G62A	hnn	45.22	-70.53	100	5.10E-03	1.49E-05	2
TA	G62A	hne	45.22	-70.53	100	-6.66E-03	4.77E-05	2
TA	G65A	hnn	45.2	-67.56	100	1.46E-01	-2.37E-04	2
TA	G65A	hne	45.2	-67.56	100	6.32E-02	-9.36E-05	2
TA	H62A	hnn	44.57	-71.16	100	3.50E-02	-7.23E-05	2
TA	H62A	hne	44.57	-71.16	100	-5.32E-02	5.38E-04	2
TA	I63A	hnn	44.05	-70.58	100	8.29E-02	-1.36E-04	2
TA	I63A	hne	44.05	-70.58	100	1.40E-01	-2.95E-04	2